Fatigue Crack Growth, Creep-Fatigue Crack Growth and Creep Crack Growth Behavior of Inconel® 740H at Elevated Temperature

A Thesis

Presented in Partial Fulfillment of the Requirements for the

Degree of Master of Science

with a

Major in Mechanical Engineering

in the

College of Graduate Studies

University of Idaho

by

Zane J. Holliday

Approved by:

Major Professor: Robert Stephens, Ph.D.

Committee Members: Gabriel Potirniche, Ph.D.; Michael Maughan, Ph.D.

Department Chair: Gabriel Potirniche, Ph.D.

May 2023

Abstract

The purpose of this study is to characterize the fatigue crack growth, creep-fatigue crack growth and creep crack growth of Inconel® 740H at elevated temperature. Tests were performed on solution annealed, heat-treated, compact tension specimens and performed in accordance with ASTM standards. Experimental tests were performed at 750°C and 800°C. Loading conditions for fatigue crack growth were 15Hz, 0.25 Hz and 1/60 Hz whereas creep-fatigue crack growth conditions included a 60s and 6s hold time. Creep crack growth tests were performed at a constant load. This study characterized crack growth rate as a function of stress intensity, K. Fractography was also performed at various ΔK and K levels. At 750°C, it was found that crack growth rates were similar with the exception of the 1/60 Hz test. For the 60s hold test, fractography revealed more extensive secondary cracking than the 1/60 Hz test, leading to potential crack tip blunting. Exploratory work was performed at 800°C and allowed for a temperature comparison as well as the evaluation of a creep crack growth test. An increase in temperature showed a change in creep-fatigue crack growth but little change in fatigue crack growth behavior for the material.

Acknowledgements

First and foremost, I would like to thank Dr. Stephens for his guidance throughout the last year and a half. He has been quick to forgive my mistakes, has challenged me to grow in the way I think and is always eager to get his hands dirty. I would also like to thank Dr. Michael Maughan and Dr. Gabriel Potirniche for their support as both teachers and mentors over the course of this degree.

Next, I would like to thank Anthony DeSantis and Michael Myers for the time they spent training and preparing me for my research. Lastly, I would like to thank Troy Hanes for pouring his time into helping me succeed, and the extra hours he sacrificed to make this research possible.

Dedication

This thesis is dedicated to my parents for their constant love and support. Mom, I'm finally willing to admit that writing is a useful skill (even for an engineer).

This work is also dedicated to Joseph Dekold, Andrew Botterbusch and Jefferey Ostlind for making the last 5 years an unforgettable experience. Your friendship will not be forgotten.

Table of Contents

List of Figures

List of Tables

Nomenclature

a	crack length
ASTM	American Society of Testing Materials
B	Specimen Thickness
CFCG	Creep Fatigue Crack Growth
C(T)	Compact Tension Specimen
da/dN	Fatigue Crack Growth Rate
da/dt	Time Rate of Crack Growth
DCPD	Direct Current Potential Drop
FCG	Fatigue Crack Growth
740H	Inconel® 740H
LEFM	Linear Elastic Fracture Mechanics
LLD	Load Line Displacement
K	Stress Intensity
K_{max}	Maximum Stress Intensity
K_{min}	Minimum Stress Intensity
ΔK	Change in Stress Intensity from Maximum to Minimum
N	Number of Applied Cycles
P	Applied Load
P_{max}	Maximum Applied Load
P_{min}	Minimum Applied Load
R	Stress ratio
SEM	Scanning Electron Microscope
t	Specimen Thickness
t_{hold}	Hold Time
W	Specimen Width
σ_{ys}	Yield Strength
γ'	Gamma Prime

1.) Introduction

The world's demand for energy continues to grow as it becomes increasingly more dependent on technology. While clean energy generation continues to grow, the International Energy Agency indicates that coal is still the largest source of electricity generation [1]. A new generation of power plants include ultra-supercritical (USC) and advanced ultra-supercritical (A-USC) coal-fired power plants which use steam to produce energy at higher efficiencies. Raising the temperatures of the boilers in these plants increases the energy efficiency with A-USC power plants showing a higher efficiency than USC power plants [2]. Boiler systems undergo high levels of pressure and temperature to produce the steam required for these power plants.

To design these boilers, it is critical to choose a material with high strength and corrosion resistance. Inconel® 740H (740H) is a nickel-based superalloy used to produce pipes and fittings for the boilers used in A-USC power plants. While there are several studies on fatigue, creep-fatigue and creep crack growth on superalloys such as Haynes 282 and Inconel® 617 (617), limited research has been performed on 740H. This study focused on fatigue crack growth (FCG), creep-fatigue crack growth (CFCG) and creep crack growth (CCG) at temperatures of 750°C and 800°C which represent conditions the material would undergo during service. The University of Idaho made a partnership with Electric Power Research Institute (EPRI) to perform this research.

2.) Literature Review

2.1 Inconel® 740H

740H is a nickel-based superalloy designed for A-USC boiler piping. This alloy was designed to operate at temperatures up to 760°C and pressures up to 35 MPa. Currently, it is approved by ASME Boiler and Pressure Vessel Code Case 2702 for operating temperatures up to 800°C (under allowable stresses). While its original design was intended for A-USC boiler tubes, it was later adapted for the use of steam headers which are connected to the boiler. Currently, advanced energy research applications fall in-between the temperature range of 700-750°C, however, there is developing interest in creep crack growth (CCG) performance at 800°C [3],[4].

740H alloy originated from Nimonic® 263 but has a higher chromium content to improve resistance to corrosion at higher temperatures (chemical composition limits are shown in Table 1). Other than its high chromium content, 740H is primarily made up of cobalt and nickel. Some competitor materials of 740H include Haynes 282 and Inconel® 617 (IN617) which will be discussed more in Section 2.3. 740H has an austenitic structure and becomes age hardened by a gamma prime (γ') phase. The γ' phase forms precipitates that align with the gamma matrix which is a face-centered cubic crystal structure. These precipitates are formed out of niobium, aluminum and titanium as the material is heat treated [4].

Table 1: 740H Chemical Composition Limits [4].

Element	Cr	Co	Al	Ti	Nb*	Fe	C	Mn	Mo	Si	Cu	P	S	B	Ni
Min.	23.5	15.0	0.2	0.5	0.5	---	0.005	---	---	---	---	---	---	0.0006	Bal
Nom.	24.5	20	1.35	1.35	1.5		0.03		0.1	0.15					
Max.	25.5	22.0	2.0	2.5	2.5	3.0	0.08	1.0	2.0	1.0	0.50	0.03	0.03	0.006	---

The yield strength, tensile strength, and elongation of 740H are shown in Table 2 for room temperature (20℃) and testing temperatures (750℃, 800℃). The material was solution annealed at 1121℃ and heat-treated at 800℃ for 5 hours.

Table 2: Material Properties of 740H in the longitudinal direction [4].

Material Properties	20℃	750℃	800℃
Yield Strength (MPa)	742	576	547
Tensile Strength (MPa)	1133	815	689
% elongation	24.3	22.9	31.5

For the purpose of scanning electron microscopy (SEM) analysis shown in Chapter 3, it is useful to understand the approximate grain size of the material. A study on the microstructure of 740H had a grain size of roughly 100 μm when measured in its as received condition (solution annealed) as shown in Figure 1 [5]. This serves as a comparison to fractography taken in Chapter 4 of this study.

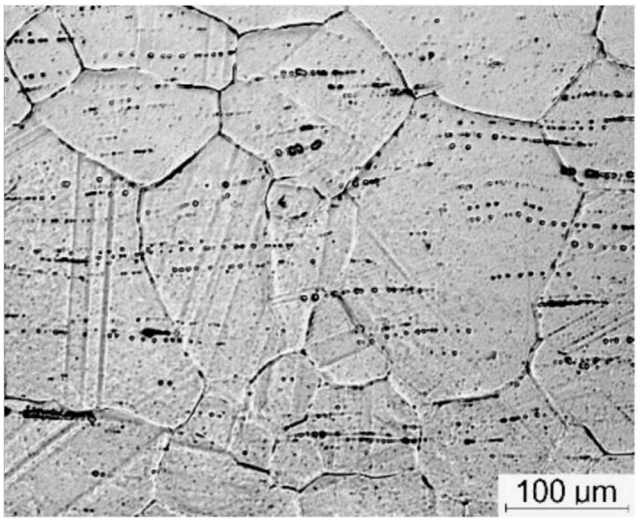

Figure 1: Average grain diameter for as-received 740H [5].

Figure 2 shows the fracture surface from a 740H creep rupture test at 750℃ and 180 MPa [6]. The fracture surface proved to be predominantly intergranular and will be used to validate the fractographic observations made in this study.

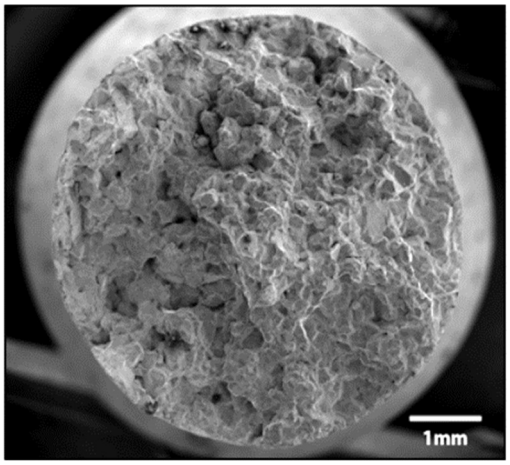

Figure 2: SEM image of fracture surface
from creep rupture test at 750℃.

2.2 Linear Elastic Fracture Mechanics (LEFM)

Fracture mechanics is the study of the strength of a component with the existence of cracks [7]. LEFM is a common way to examine crack growth under fatigue loading. LEFM requires an assumption that the material behaves in a mostly linear elastic manner. For materials that fail this assumption, other methods such as elastic-plastic fracture mechanics are used. LEFM is effective from the start of a noticeable crack to the fracture of the component [7]. In LEFM, there are three primary modes of loading. Mode I is the opening mode, Mode II is considered In-plane shear, and Mode III is out-of-plane shear as shown in

Figure 3. For this study, all tests were performed and evaluated under Mode I loading conditions.

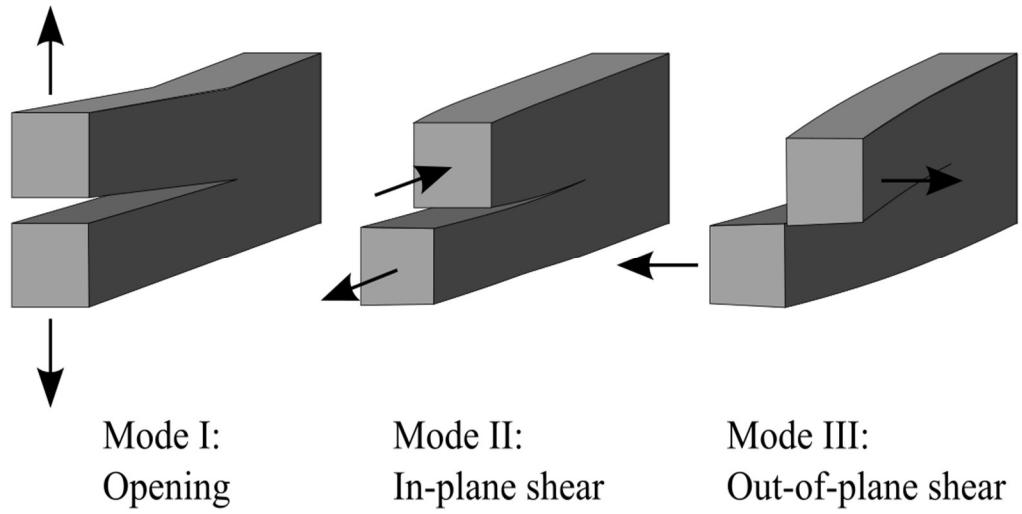

Figure 3: Three modes of loading in LEFM [8].

A notable factor in LEFM is the stress intensity factor denoted as K. This factor was developed by Alan Griffith, often considered "The Father of Fracture Mechanics." Griffith developed an equation that relates the far field stress with the square root of the crack length [7]. This equation was first used for brittle materials like glass. Later on, George Irwin took Griffith's theory and applied it to metals, proving that the crack tip driving force could be characterized by the stress intensity factor K. Irwin made this discovery by recognizing that the plastic zone at the crack tip drives crack growth and fracture of the component [7]. A general form of Griffith's equation is shown in Equation 1 where the variables include the crack length (a) and the far field stress (S).

$$K=S\sqrt{\pi a} \quad (1)$$

In fatigue crack growth testing, ΔK is described as the change from maximum stress intensity (K_{max}) to minimum stress intensity (K_{min}) as shown in Equation 2. ΔK is extremely valuable in FCG and CFCG testing because it allows for an accurate fatigue crack growth rate comparison for creep-brittle materials.

$$\Delta K = K_{max} - K_{min} \tag{2}$$

For this study, compact tension (C(T)) specimens were used for all FCG, CFCG and CCG testing. According to the American Society for Testing and Materials (ASTM) Standard E-647 [9], K for a compact tension (C(T)) specimen is calculated in Equation 3,

$$K = \frac{P}{BW^{\frac{1}{2}}} F(\alpha) \tag{3}$$

where P is the applied load, B is the specimen thickness, W is the specimen width, and F (α) is a geometric factor calculated from the crack length and width of the specimen (α=$\frac{a}{W}$) with Equation 4 [9].

$$F(\alpha) = \left[\frac{(2+\alpha)}{(1-\alpha)^{\frac{3}{2}}}\right](0.886 + 4.64(\alpha) - 13.32(\alpha)^2 + 14.72(\alpha)^3 - 5.6(\alpha)^4) \tag{4}$$

Measuring the crack length during crack growth at elevated temperature can be challenging as the tests are performed inside a furnace. Therefore, the crack length of a specimen can be determined by using a linear relationship between crack length and direct current potential drop (DCPD) a technique that correlates crack length to a voltage change in the specimen as

the crack grows. Figure 4 shows an example of this linear relationship for a 740H (0.25 Hz) test that was conducted in this study.

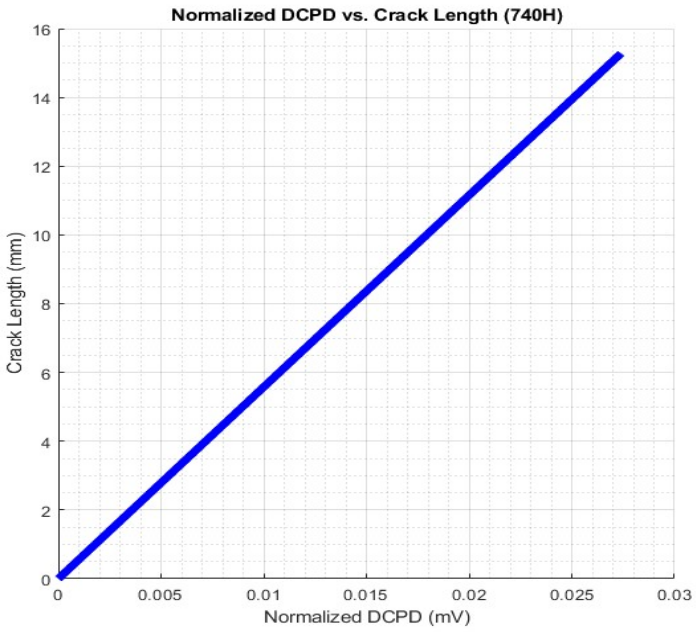

Figure 4: Linear relationship between crack length and DCPD.

The equation to relate these two variables is shown in Equation 5, where a_0 and a_f are the initial and final crack lengths, V_0 and V_f are the initial and final DCPD values, and V is the instantaneous DCPD value [9].

$$a = a_0 + (a_f - a_0) \times \frac{V - V_0}{V_f - V_0} \tag{5}$$

The crack growth rate for fatigue testing can be described as the change in crack length divided by the change in cycles. The ASTM standard E-647 [9] suggests using what is referred to as the secant method to calculate the crack growth rate from an a vs. N curve. This method is also known as the point-to-point technique and was used to average the data

collected as shown in Equation 6. To compare the crack growth rate accurately, the average crack length was used to calculate ΔK [9].

$$\frac{da}{dN} = \frac{a_{i+1} - a_i}{N_{i+1} - N_i} \tag{6}$$

For CCG and CFCG testing, K_{max} can be compared to crack growth rate as a function of time rather than cycles. A CFCG test can be represented with both types of crack growth rates (da/dN, da/dt) as shown in Equation 7 where t_{hold} is the hold time on the specimen.

$$\frac{da}{dt} = \frac{\frac{da}{dN}}{t_{hold}} \tag{7}$$

2.3 Comparable Alloys to 740H

With limited FCG, CFCG and CCG data for 740H, understanding how 740H compares to its competitors is paramount. Superalloys Haynes 282 and Inconel® 617 (617) are other nickel-based alloys that have been used in similar coal-fired power-plant applications to 740H. Some crack growth studies have been done for both Haynes 282 and 617 which serve as a comparison to the results from this study.

Haynes 282 is a γ’ strengthened superalloy known for its creep strength and fabricability. Comparing material composition shows that 740H has a higher weight % of chromium and cobalt while Haynes 282 has a higher weight % of titanium [10]. A study at Oregon State University in 2015 was performed to understand the FCG behavior of Haynes 282 [11]. Figure 5 shows the data for crack growth rate as a function of ΔK for frequencies of 0.25 and 25 Hz at various temperatures.

At 750°C, the 0.25 Hz test shows a significant shift in crack growth rate from 25 Hz with less resistance to crack growth. Temperature comparison shows that an increase in temperature leads to an increase in the crack growth rate. Fractography of the specimens showed transgranular failure with minimal evidence of intergranular cracking. Further discussion with this alloy will be covered in Chapter 4 as a comparison to the results for 740H.

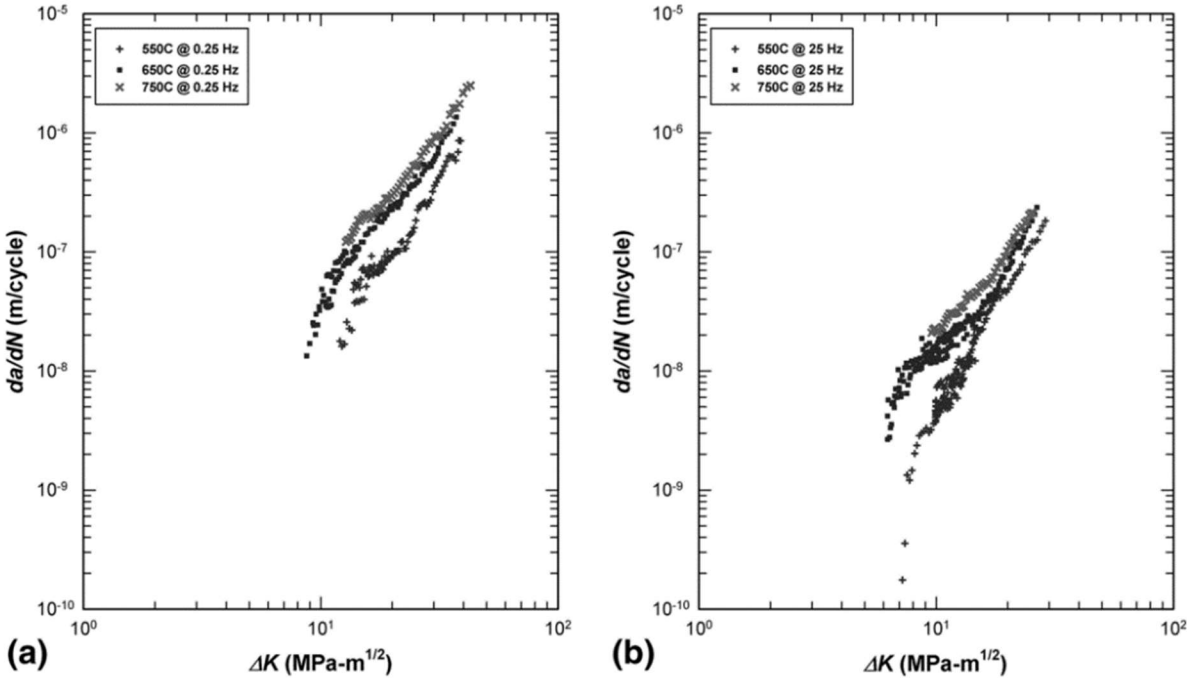

Figure 5: FCG testing at 0.25 Hz and 25 Hz for T=550°C,650°C and 750°C [11].

Alloy 617 is another nickel-based alloy that is comparable to 740H. While it is strengthened by precipitation of the γ' phase, it proves to have a lower tensile strength and yield strength than 740H. 617 has a higher content of molybdenum whereas 740H contains a higher nickel content. Figure 6 shows an allowable stress vs. temperature comparison of 617 and 740H, showing the superior strength of 740H at moderate temperature with a convergence at roughly 800°C.

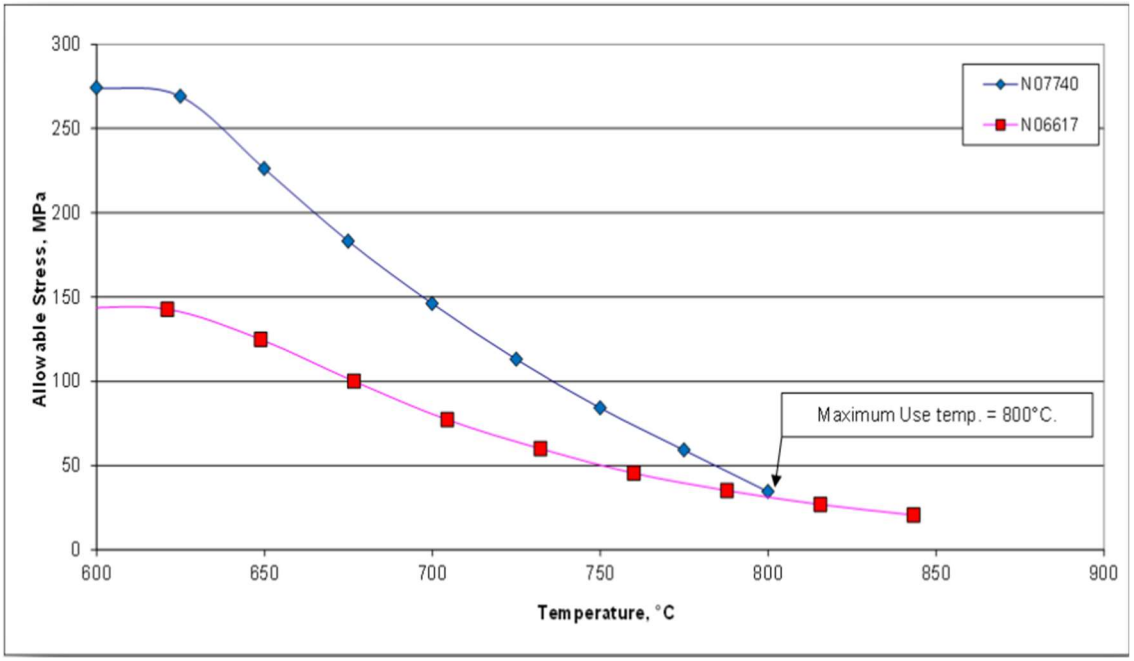

Figure 6: Comparison of ASME section I allowable stresses for alloy 617 and alloy 740H [4].

Figure 7 shows a material savings comparison for 740H vs. 617 where the quantity of 740H is one-half of the quantity 617 used for a double main steam (MS) and hot reheat system (HRH). 740H also allows for the construction of a single MS and HRH option (due to lower flow stress at extrusion temperatures) [4],[12]. This shows that less material is required for boiler systems made from 740H.

A fatigue and creep-fatigue crack growth study on IN617 was conducted in 2013 by the Idaho National Laboratory (INL) at temperatures 650°C and 800°C [13]. Results showed time-dependent crack growth for both FCG and CFCG tests with primarily intergranular

cracking and signs of secondary cracking occurring perpendicular to the fracture plane. It should be noted that these tests were performed at a load ratio of R=.05 [13].

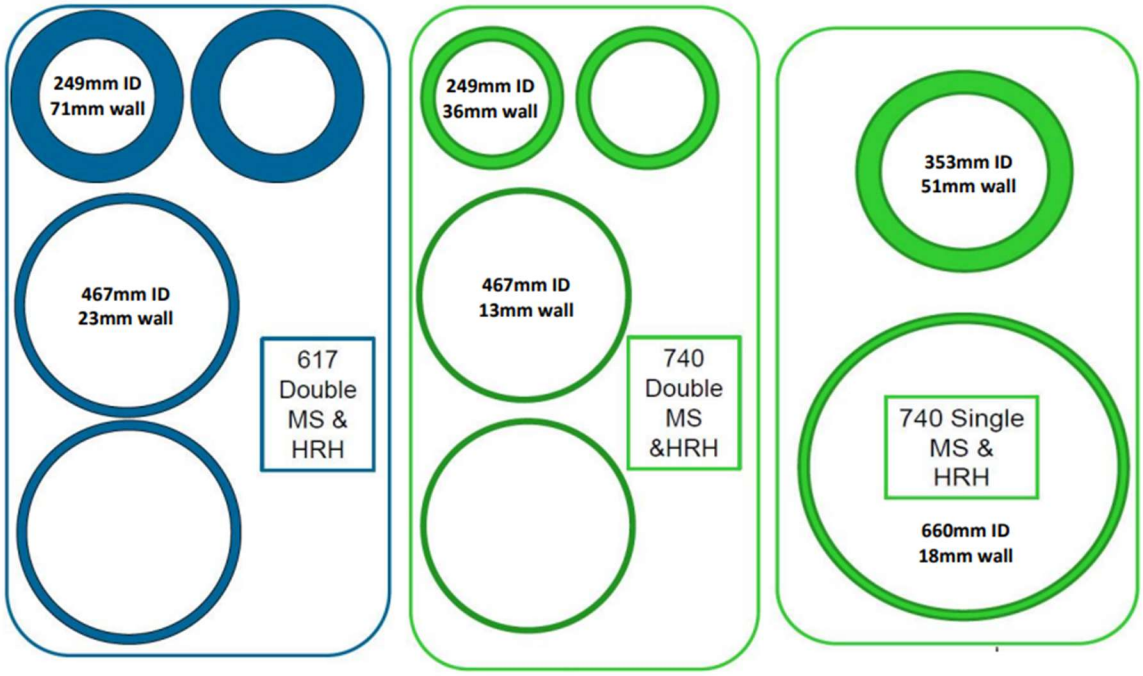

Figure 7: Material savings comparison with a double MS and HRH system and a single MS and HRH [4].

2.4 Creep Brittle vs. Creep Ductile

In fracture mechanics it is important to understand the difference between creep-ductile and creep-brittle materials. Some common creep-brittle materials include aluminum alloys, nickel-based superalloys, and ceramics, whereas many steels are creep-ductile. Creep-brittle materials experience small-scale creep where the creep zone is small compared to the crack length and geometry of the body. This allows for use of K_{max} and ΔK to characterize the crack growth rate of the material. On the other hand, creep-ductile materials require $C_{t,\,avg}$ and C* as parameters for materials that have extensive creep zones extending past the plastic

zone diameter of the crack tip [14]. For this study, the K parameter was used due to the creep-brittle nature of nickel-based superalloys.

A study was performed by Yokobori [15] in order to validate whether a material behaves in a creep-brittle or creep ductile manner. Yokobori compared the change in crack length (Δa) vs. non-dimensional time (t/t_f) to determine whether the material demonstrates uniform velocity or acceleration. Creep-brittle materials are dominated by uniform velocity whereas creep-ductile materials are dominated by uniform acceleration. Yokobori showed that IN100 (a creep-brittle material) demonstrated uniform velocity for 80% of its life whereas Cr-Mo-V steel (a creep-ductile material) experienced acceleration for 60% of its life.

For creep-fatigue crack growth, the total crack growth rate can be written as both a cycle and time dependent part as shown in Equation 8. Creep deformation during the hold time is typically limited for time-independent materials [14]. For creep-ductile materials, time-dependent crack growth rate is dominant for long hold times as the creep zone increases.

$$\left(\frac{da}{dN}\right)=\left(\frac{da}{dN}\right)_{\text{cycle}}+\left(\frac{da}{dN}\right)_{\text{time}} \tag{8}$$

3.) Experimental Details

3.1 Material and Specimen Geometry

740H specimens for these experiments were removed from an existing large pipe segment. The pipe was solution annealed; a common method used to treat nickel-based superalloys. The solution annealing treatment was used to bring the specimen into a single-phase structure and was air-quenched to dissolve unwanted precipitates [16]. All specimens were heat-treated at 800℃ for 4 hours to ensure that the specimens were age hardened by the precipitation of γ'.

Specimens were machined into C(T) specimens and were sized in accordance with ASTM standards for FCG, CFCG and CCG testing [9]. The purpose of a C(T) specimen is to provide a standardized geometry that can allow for accurate comparison between materials. The geometry of the C(T) specimen used is shown in Figure 8 where W=50.7 mm and B=12.7 mm. Details of the notch cut in the specimen were created using electric discharge machining (EDM). The length from the load line of the specimen (where the pin holes are centered) to the end of notch is a_n = 10.2 mm and is considered the starting crack length.

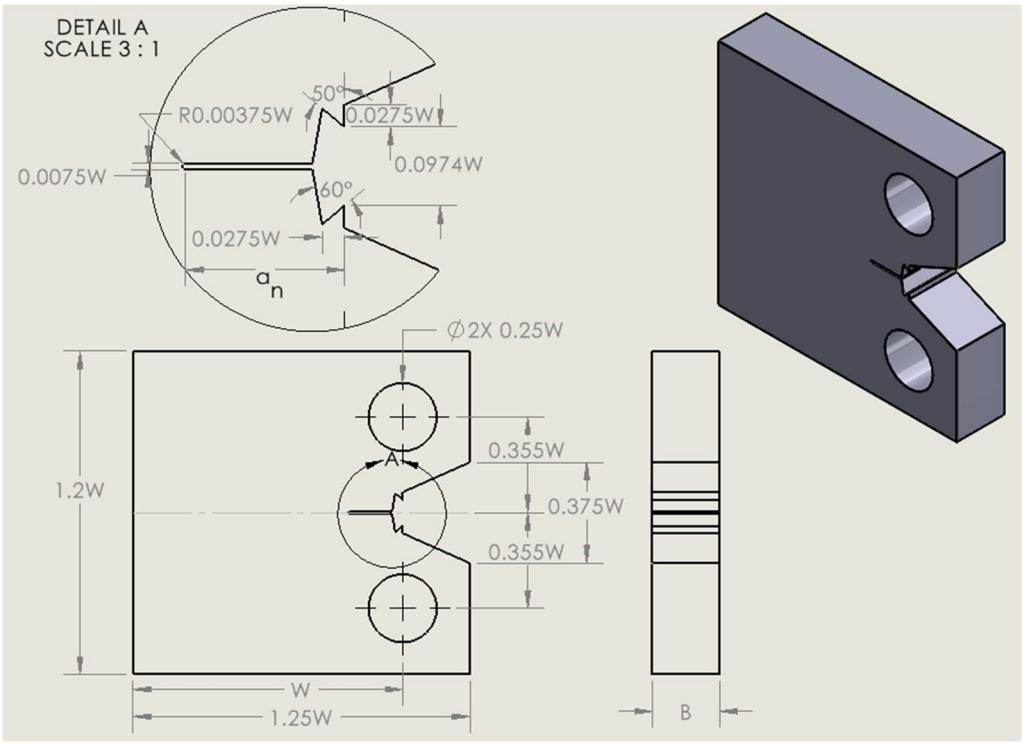

Figure 8: C(T) specimen geometry with machined notch.

3.2 Experimental Testing Equipment

All specimens were heat-treated as summarized in Section 3.1 using an evenheat Rampmaster ® Model RM3 and an Applied Test Systems ® (ATS) split case furnace. Specimens were then polished to a 1µm grit on a rotary table which allowed the user to measure the crack length visually during testing.

All FCG and CFCG tests were performed on a servo-hydraulic load frame MTS 312.11 as shown on the left in Figure 9. This frame has a load capacity of 10 kips and was controlled by a MTS 458.20 MicroConsole. All tests were performed at elevated temperatures of 750°C and 800°C using an ATS split case furnace. The temperature was controlled using a Watlow ® EZ-Zone PID temperature controller.

For the CCG test, a creep frame was fabricated that used a 30:1 lever arm for specimen loading. This frame held the specimen at a constant load and was loaded by placing weights in a hanging container as shown on the right in Figure 9. An Optima ® OP-312 load cell was placed in series with the load train to measure the load applied to the specimen. An ATS split case furnace was used to heat the specimen and used a Twidec ® PID temperature controller. Two dial indicators were used to verify extensometer measurements and were located near the top rail of the frame in the front and back. The grips, rods, and pins for the servo hydraulic frame and the creep frame were constructed out of IN718 which is a high strength nickel-based superalloy, commonly used for high temperature material testing.

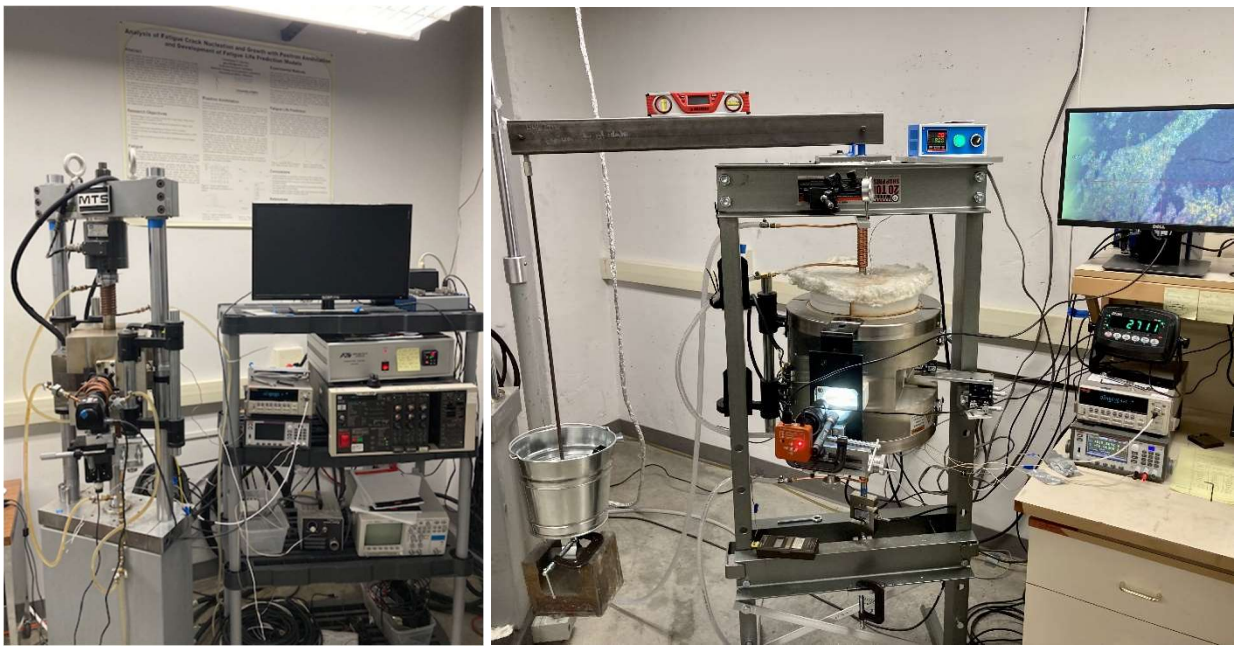

Figure 9: FCG frame on the left and CCG frame on the right.

An MTS ® model 632.11B-20 extensometer was modified to accept ceramic rods that rest in the specimen knife edges and was used to evaluate the crack opening displacement (COD) and load line displacement (LLD). Voltage output from the extensometer was conditioned through the MTS ® 458.20 MicroConsole. Figure 10 shows the modified extensometer used for all tests.

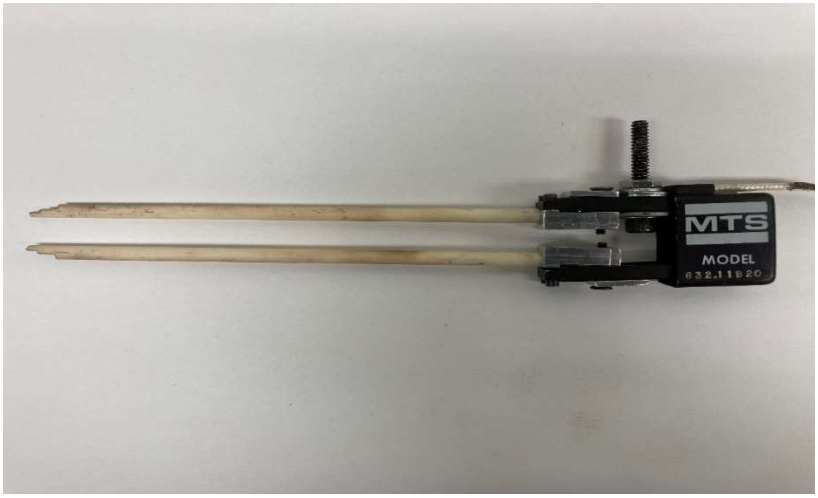

Figure 10: MTS extensometer used for all FCG, CFCG, and CCG testing.

DCPD data was collected using a Keithley ® 2182A Nanovoltmeter. A power supply of 18V and 2A was specified using a Keithley ® 2280S-32-6 Precision Measurement DC Power Supply. Each C(T) specimen was wired at spot weld locations shown in Figure 11 using a WhichiTech ® spot welder. B+ and B- are the DCPD wires and were wired on each side of the specimen using 26-gauge wire. The power supply was wired with 22-gauge wire at A+ and A-. The thermocouple used for the temperature controller was welded near the middle of the specimen (just off the crack plane).

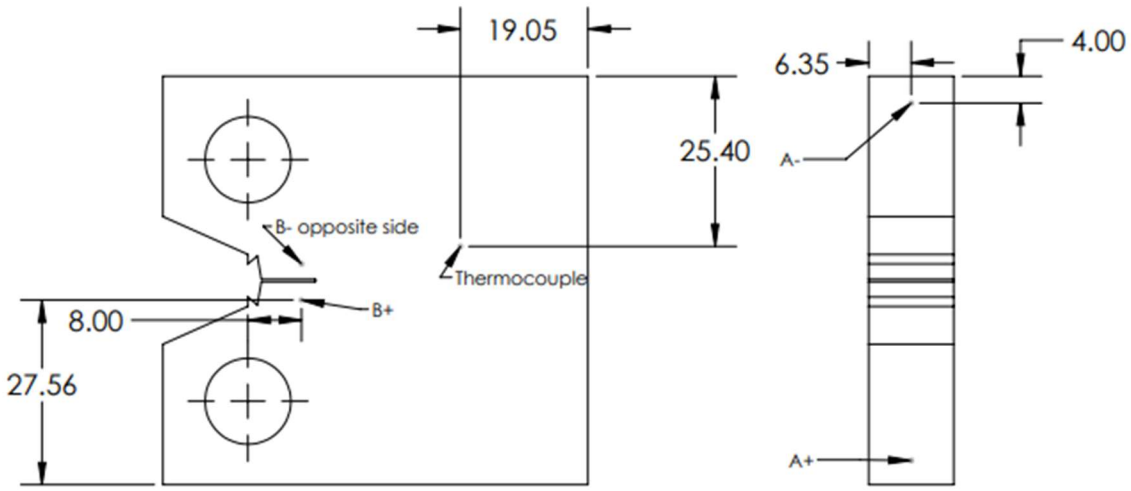

Figure 11: Spot weld locations for DCPD, power supply and thermocouple (in mm).

3.3 Experimental Procedure

All specimens were pre-cracked using the servo-hydraulic load frame at frequencies of 15-25 Hz. Pre-cracking was performed at room temperature in accordance with ASTM standards. All fatigue pre-cracking was performed at a load ratio of R=0.1 (R is represented in Equation 9) which grew the crack to a desired starting K or ΔK. All pre-cracking was performed through the process of load shedding (every 0.5 mm of crack growth) which allowed for the crack to grow without introducing an excessive plastic zone. More information on the load shedding procedure can be found in Appendix A.9.

$$R = \frac{P_{min}}{P_{max}} \tag{9}$$

After each specimen was pre-cracked, the furnace was brought to the desired elevated temperature. Tests were performed at R=0.1 and the respective waveform was created with the MicroConsole. FCG tests included a 15 Hz sinusoidal waveform with 0.25 Hz and 1/60

Hz tests using a triangular waveform (waveforms shown in Table 3). CFCG tests were performed at hold times of 60 seconds and 6 seconds.

Table 3: Specimen testing matrix.

Specimen ID:	Temperature °C	Loading Waveform	Hold Time/Frequency
740-1	750	Sinusoidal	15 Hz
740-2	750	Triangular	0.25 Hz
740-3	750	Trapezoidal	60s
740-4	750	Trapezoidal	6s
740-5	750	Triangular	1/60 Hz
740-6	800	Triangular	1/60 Hz
740-7	800	CCG	N/A
740-8	800	Trapezoidal	60s

It is important to understand the difference between the slow frequency test 1/60 Hz and the 60s hold test. While both tests shared the same maximum and minimum loads and were loaded under the same time period, the 60s hold test held the maximum load for 59.5s before a single cycle was applied (each loading and unloading time was 0.25 seconds). Likewise, the 6s hold test was held at 5.5 seconds before cycling. The difference between these waveforms can be seen in Figure 12.

The primary form of data collection was performed using an NI data acquisition (DAQ) instrument which interfaced with a data collection software. The data was recorded at 5 Hz for FCG and CFCG tests and 1 Hz for the CCG test. Values collected include DCPD, LLD, and time. Data were also collected manually regarding instantaneous DCPD output, cycle count, and visual crack length of the specimen. The visual crack length was determined with the use of a camera measurement system which served as a backup for gaps in data

collection. Some of these potential gaps include power outages, equipment issues and unexpected computer updates.

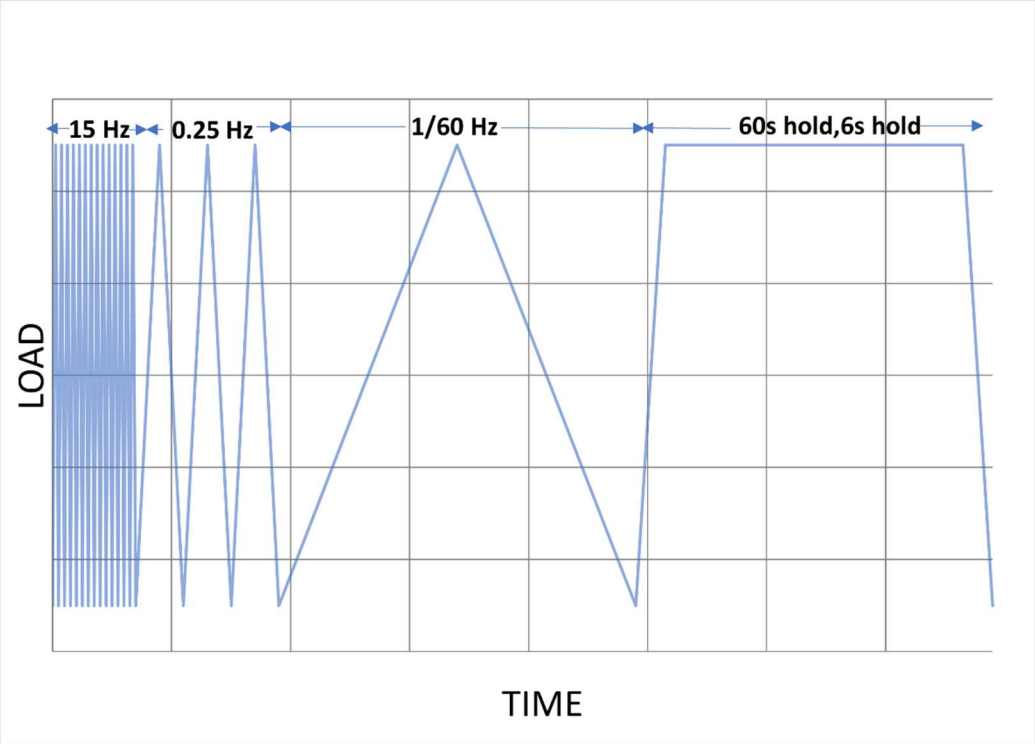

Figure 12: Loading waveforms for FCG and CFCG tests.

As the specimen approached fracturing into two pieces, the test was stopped, and the load was brought to zero. The furnace was opened to allow the specimen to cool. The specimen was then fatigued to fracture. After the specimen was broken into two pieces, the user was able to view the crack front and determine the initial crack length (a_i) and final crack length (a_f) using a microscope as shown in Figure 13.

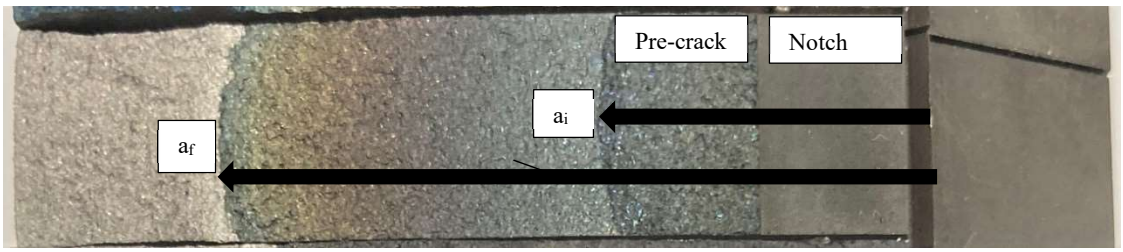

Figure 13: Fracture surface of 740-2 with crack growth from right to left.

4.) Results and Discussion

4.1 FCG and CFCG at 750°C

The test matrix developed for this research included FCG and CFCG testing at 750°C. This temperature was chosen because it reflects the advanced energy application of 740H. Five tests were performed at 750°C, as shown in Table 4.

Table 4: Summary of FCG and CFCG results at T=750 °C

Specimen ID	Waveform	a_o (mm)	a_f (mm)	ΔK_o (MPa√m)	ΔK_f (MPa√m)	N (cycles)	Duration (hours)
740-1	15 Hz	14.96	38.21	19.24	102.46	89000	1.7
740-2	0.25 Hz	18.48	38.54	19.30	89.71	45664	50.7
740-3	60s Hold	22.48	37.76	31.52	107.47	24513	409
740-4	6s Hold	18.686	36.96	23.47	88.76	75617	126
740-5	1/60 Hz	18.06	38.06	21.80	97.31	31757	529

A sinusoidal waveform at a frequency of 15 Hz (740-1) was chosen for the first test to serve as a baseline FCG test for the rest of the study. The specimen was pre-cracked to approximately ΔK_o = 19 MPa$\sqrt{m}$ and ended at approximately ΔK_f = 102.5 MPa$\sqrt{m}$. Due to unexpected fracture at the end of the test, the maximum DCPD value was used to determine the final crack length of the test.

A slower frequency FCG test at 0.25 Hz (740-2) was performed to evaluate any frequency effect on the FCG rate and to provide a comparison to competitor alloy Haynes 282. This test was started at approximately ΔK_o = 19 MPa$\sqrt{m}$ and ended at roughly ΔK_f = 90 MPa$\sqrt{m}$. Comparison of these two tests (740-1 and 740-2) showed that there was little change in the crack growth rate as a function of ΔK as shown in Figure 14.

Interestingly, this behavior was significantly different than the FCG data generated on Haynes 282 [11] which showed a shift in the FCG curve when going from a frequency of 25 Hz to 0.25 Hz. Comparing data in Figure 14, the Haynes 282 at 25 Hz behaved similar to 740H at 15 Hz, however, the 740H data showed little difference between the 15 Hz and 0.25 Hz tests. As a result, 740H showed better resistance to crack growth compared to Haynes 282 at the slower frequency of 0.25 Hz (for 750°C).

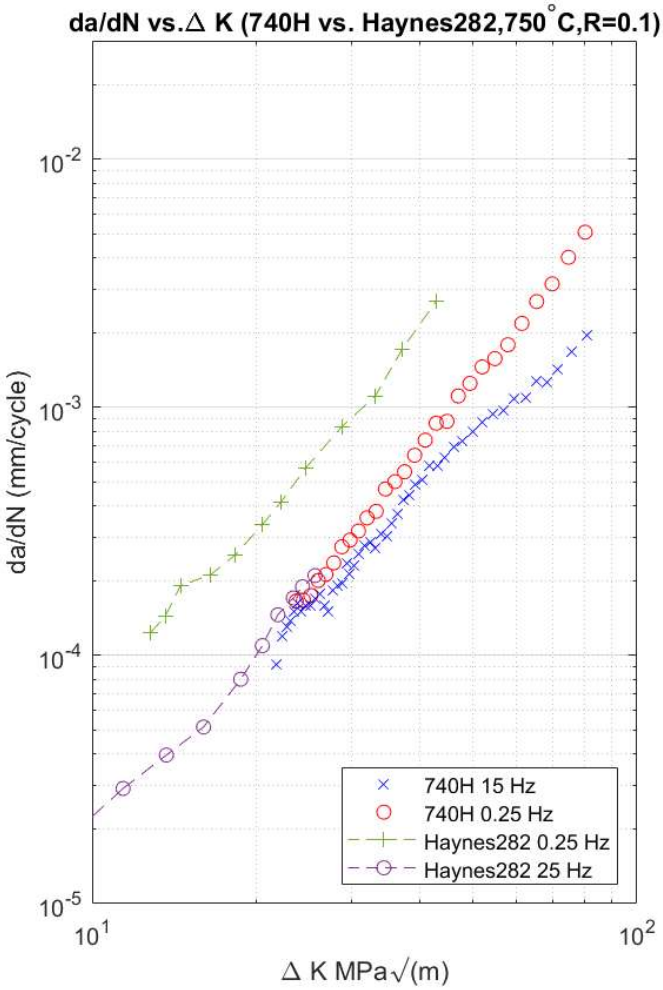

Figure 14: FCG comparison of Haynes 282 [11]and 740H at 750°C.

To observe any creep-effect on 740H, a CFCG 60s hold test (740-3) was performed starting at a similar ΔK_o as the first two FCG tests. However, several attempts to grow the

crack at this initial ΔK_o were unsuccessful as crack arrest occurred at all $\Delta K < 30$ MPa$\sqrt{m}$. The initial ΔK_o was continually increased until crack growth occurred at approximately ΔK_o = 32 MPa$\sqrt{m}$ (refer to Appendix A.3 for more information). This test terminated at roughly ΔK_f = 107 MPa$\sqrt{m}$. When comparing the 60s hold,15 Hz and 0.25 Hz tests, it was found that the 60s hold made no noticeable difference on the crack growth rate of the material. This comparison is shown in Figure 15.

A CFCG 6s hold test (740-4) was performed to evaluate the CFCG behavior at a shorter hold time. Similar to the 60s hold, the crack did not initially grow at the starting ΔK_o and the load had to be increased. The crack eventually started to grow at approximately ΔK_o = 23.5 MPa$\sqrt{m}$ and ended at approximately ΔK_f = 89 MPa$\sqrt{m}$. Data was compared to the other three tests, and it was determined that the creep-effect made little difference. This is shown in Figure 15.

One final test was performed at a slow frequency of 1/60 Hz (.016667 Hz). This was performed to gather insight into how a slow frequency FCG test compares to the 60s hold CFCG where both tests have the same time period. The test experienced some crack arrest (no crack growth) at the initial ΔK_o similar to the previous CFCG tests. However, crack growth started at approximately ΔK_o = 22 MPa$\sqrt{m}$. This proved to be a lower starting value than both the 60s hold and the 6s hold and ended at approximately ΔK_f = 97 MPa$\sqrt{m}$. The data for the 1/60 Hz test showed a noticeable shift as compared to both the 60s hold and all other tests performed at 750°C. This shift showed that adding a hold time (60s and 6s) actually increased the resistance to crack growth with the slower frequency 1/60 Hz test showing higher crack growth rates than both the CFCG and the faster FCG rates as shown in

Figure 15. On average the crack growth rate for the 1/60 Hz test was three times faster than the 60s hold test. It should be noted that significant secondary cracks were observed on the fracture surface of the 60s hold test which may have decreased the driving force of the crack tip. More discussion on this is included in Section 4.4. It should also be noted that a hook is formed at the beginning of the curve for the 60s hold test. This behavior could be attributed to the transient region which occurs when steady-state conditions for crack growth are not yet reached [17]. As a result, for the data associated with a hook, K may not be sufficient for characterizing the crack growth rate. It is also possible this behavior is attributed to the actual

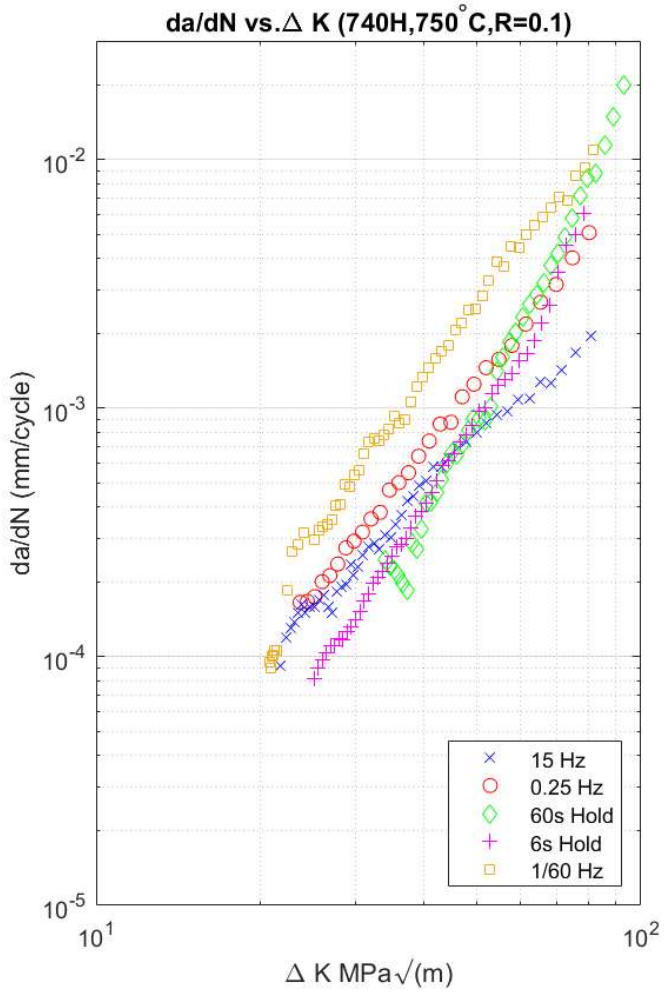

Figure 15: FCG and CFCG at 750℃.

crack growth of the 60s hold test. This means that the crack growth rate at the initial ΔK may decrease as crack growth begins. Comparing the 1/60 Hz slow frequency test from Figure 15 to the 0.25 Hz test for Haynes 282 from Figure 14 showed that 740H continues to have superior crack growth resistance.

Comparing FCG and CFCG of 740H to IN617, results from this study show that 740H is primarily a time-independent material, whereas crack growth in IN617 was found to be primarily time dependent for FCG and CFCG [13]. While the two materials are similar in composition, this shows that 740H is dominated primarily by cycle-dependence.

4.2 FCG, CFCG and CCG at 800℃

During the course of this study, the sponsor of this research suggested exploratory (CCG) testing at 800℃ to determine temperature effects and understand how the CCG behavior of 740H would be affected at its maximum allowable temperature. Due to age-hardening of all specimens at 800℃ prior to testing, it was assumed that the testing matrix at 750℃ would differ from testing at 800℃. This is because γ' precipitates could begin coarsening as grain boundary decohesion was accentuated at 800℃. To make an accurate FCG and CFCG comparison, two tests were run: a 1/60 Hz FCG test and a 60s hold CFCG test. Results from all three tests at 800℃ are shown below in Table 5.

Table 5: Summary of FCG, CFCG and CCG results at T=800℃.

Specimen ID	Waveform	a_o (mm)	a_f (mm)	ΔK_o (MPa√m)	ΔK_f (MPa√m)	N (cycles)	Duration (hours)
740-6	1/60 Hz	18.06	36.16	20.36	72.52	25541	426
740-7	CCG	30.08	36.13	K_{max}=55.24	K_{max}=96.15	N/A	192
740-8	60s Hold	22.40	27.35	30.39	40.86	7739	129

The slow frequency test of 1/60 Hz (740-6) started at approximately ΔK_o=20 MPa$\sqrt{m}$. The test was temporarily shut down at 24,647 cycles due to failure in one of the heating elements in the furnace. After repair, the test was continued and ended at approximately ΔK_f= 72.52 MPa$\sqrt{m}$. Details of this test can be found in Appendix A.6.

The 60s hold test (740-8) was started at a ΔK_o = 30.39 MPa$\sqrt{m}$, similar to the starting condition for 740-3 (the 60s hold test at 750°C). While data collection was limited, Figure 16 shows that the 60s hold had better resistance to crack growth than the 1/60 Hz test. A hook is seen in the 60s hold curve showing similar behavior to the 60s hold test at 750°C. The test

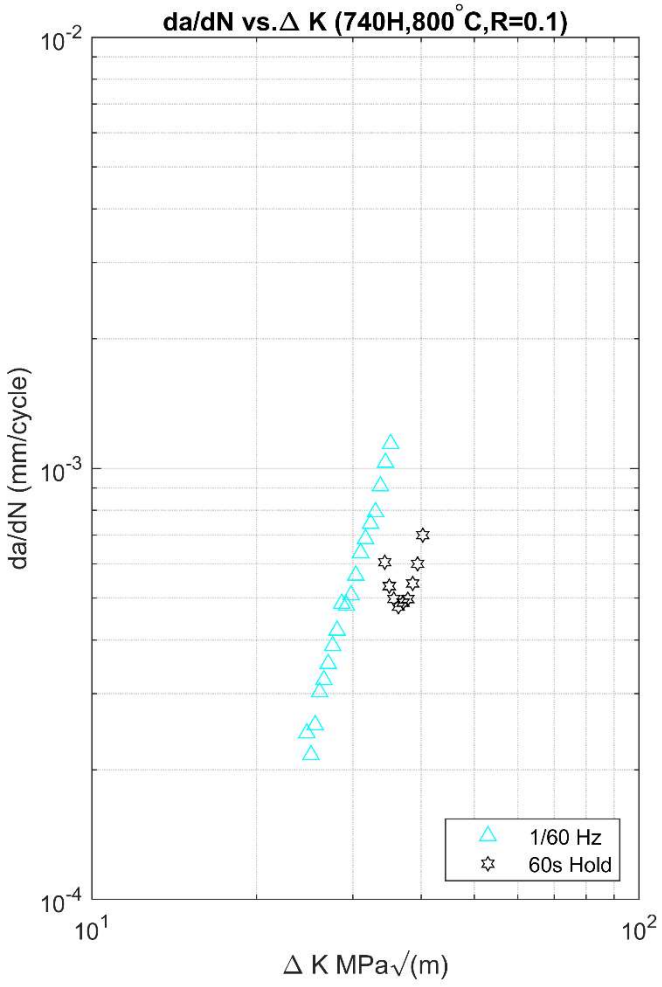

Figure 16: FCG and CFCG of 740H at 800°C.

was abruptly ended at ΔK_f=40.86 MPa$\sqrt{m}$ due to shearing of a grip pin and damage to the grips. Severe creep deformation occurred in both the grips and pins when simultaneously running the 60s hold and CCG tests on two separate test frames (damage shown in Figure 17). A study on creep rupture of IN718 (which the grips and pins were made of) showed that at approximately 100 MPa and 800℃, the creep rupture time was 174 hours [18]. The pin in this study experienced shear stress of approximately 97 MPa and failed in 129 hours. Interestingly, the slow frequency 1/60 Hz test at 800℃ showed little deformation in the pin, verifying the poor creep performance of IN718 at 800℃. All future tests above 750℃ should require the use of a higher creep resistant material such as Waspalloy, Rene 41 or cast Mar M246/M247.

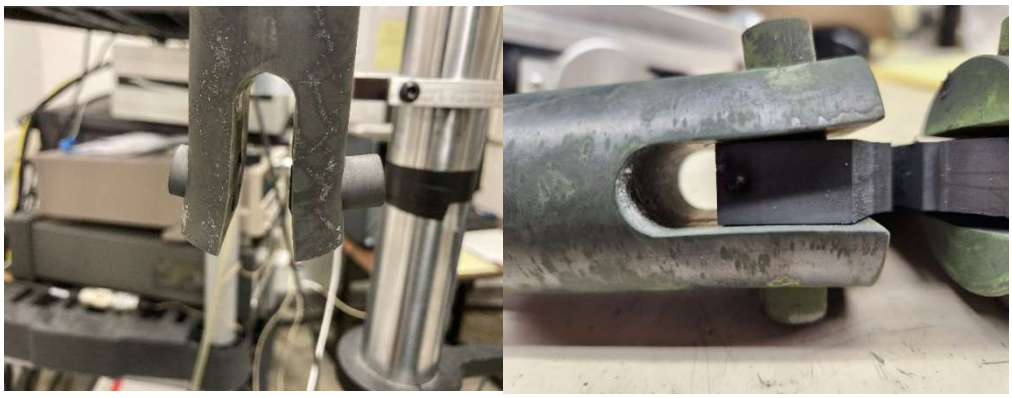

Figure 17: Inconel 718 sheared pin and deformed grips on FCG and CCG frames.

The specimen used for the exploratory CCG test (740-7) was briefly overheated to roughly 1200℃ due to a thermocouple wiring issue. While it was originally going to be started at K_{max} =30 MPa$\sqrt{m}$ (to compare with other CCG testing on similar materials), the specimen was started at K_{max} =55 MPa$\sqrt{m}$ to gain a better understanding of how 740H behaves under CCG. Future testing will require a starting K_{max} =30 MPa$\sqrt{m}$ to serve as a true

comparison to C-263 and 617. Significant creep deformation on the 740H specimen occurred which required the test to be paused several times as the lever arm on the creep frame deflected significantly and had to be adjusted. The creep deformation on the specimen that occurred showed a significantly greater crack opening displacement (COD) than all other testing in this study (extensometer data was skewed from rapid deformation). While it was difficult to visually see crack growth during the majority of the test, the fracture surface of the specimen showed crack tunneling and over 6 mm of crack growth was measured (ending at approximately K_{max} = 96 MPa$\sqrt{m}$). There was also visual evidence of gross plasticity and specimen tearing without significant crack extension on the surface as shown in Figure 18 (images taken at different magnifications). The crack tunneling behavior observed was significantly higher than all other tests in this study and will be discussed more in Section 4.4.

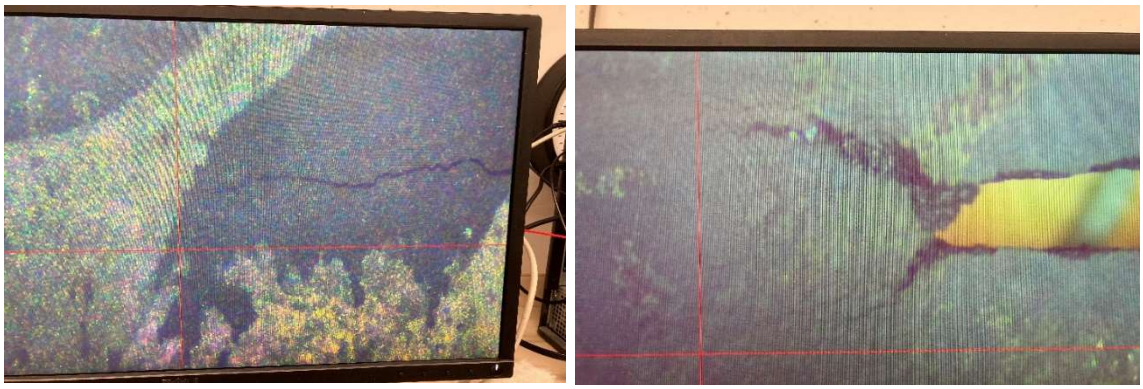

Figure 18: Images taken from the camera monitor showing visual crack growth of 740-7. Start of test on the left and end of the test on the right.

4.3 750°C vs. 800°C comparison

Figure 19 shows all FCG and CFCG test data for this study in terms of da/dN vs. ΔK. A temperature comparison can be made for both the CFCG 60s hold tests and the FCG 1/60 Hz tests. For the FCG tests at 1/60 Hz, the data at 800°C proved to compare closely with the

data at 750℃ with a slightly faster growth rate at the upper end of the curve. Comparing CFCG testing for the 60s hold showed that the data at 800℃ had a higher crack growth rate than at 750℃ (for a given ΔK) showing that CFCG resistance was worse at 800℃ than at 750℃. Increasing the temperature encouraged faster intergranular growth for the 60s hold times but appeared to have little effect on the 1/60 Hz tests. Section 4.4 includes more discussion on this shift in crack growth rate as it relates to fractography.

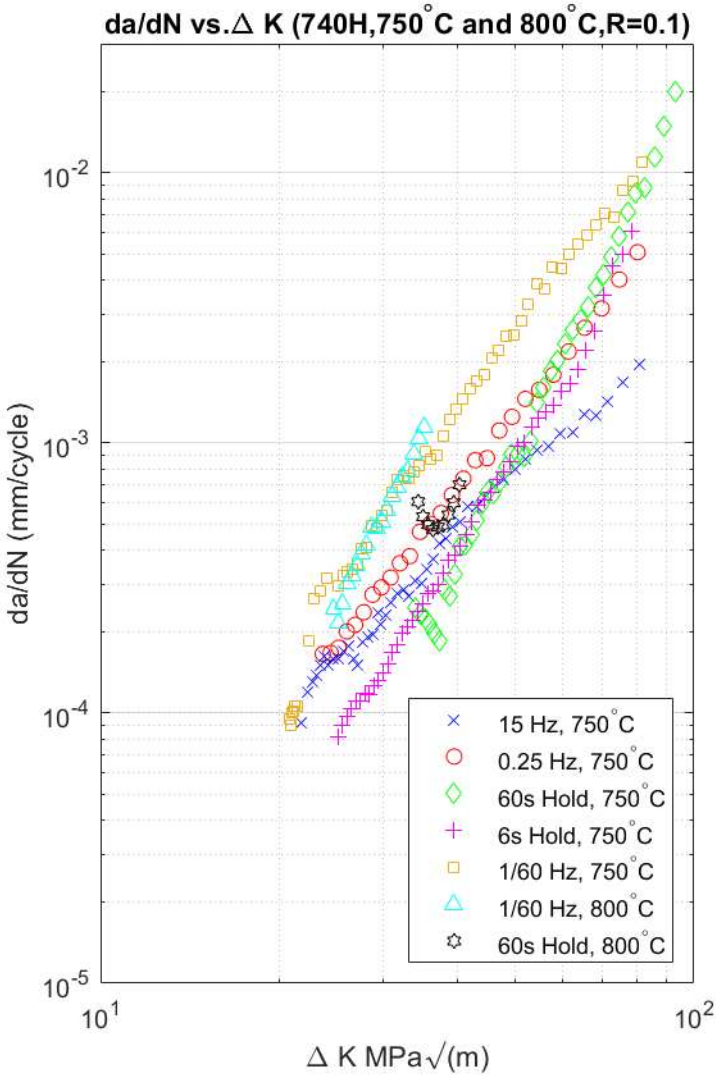

Figure 19: da/dN vs. K for all FCG and CFCG tests of 740H in this study.

A comparison of all CFCG tests with crack growth rate as a function of time (da/dt) is shown in Figure 20. Interestingly, the curves for da/dt vs. K_{max} do not correlate whereas the same curves plotted as da/dN vs. ΔK showed good overlap. The 6s hold test shows a faster da/dt than the 60s hold which agrees with cycle-dependent crack growth. This behavior shows that 740H has primarily time-independent crack growth. While some data was collected for the CCG test at 800°C, deformation in the grips and specimen showed unrealistic crack growth rates.

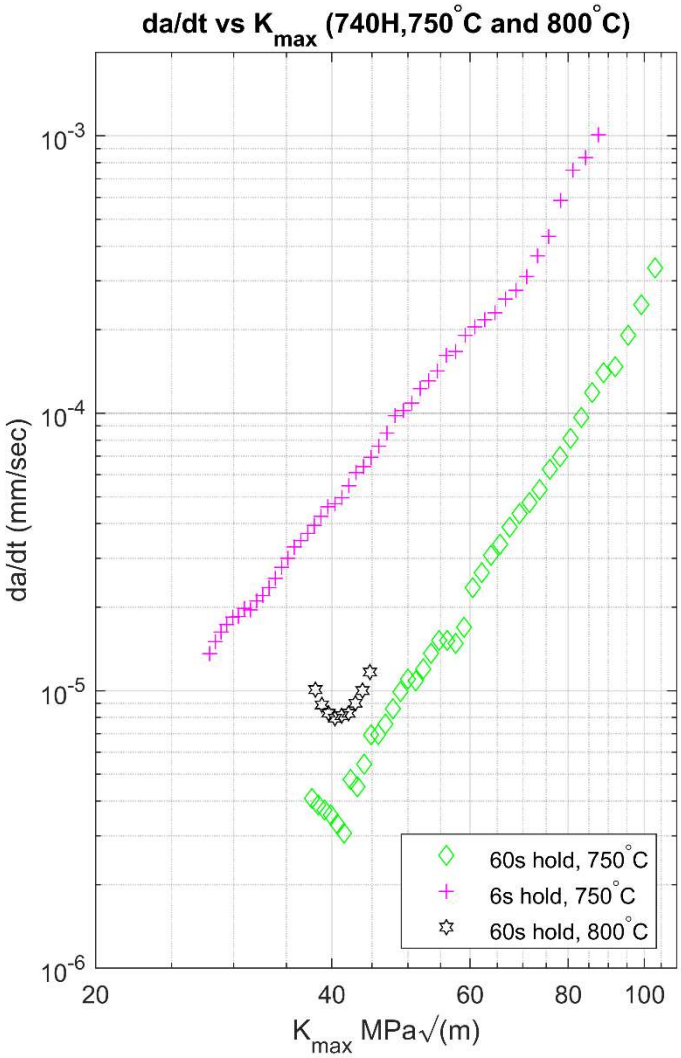

Figure 20: da/dt vs. K_{max} for CFCG at 750°C and 800°C.

4.4 Fractography

Fractography was performed on the fracture surface of each specimen with the exception of 740-8 (the 60s hold test at 800℃). The fracture surfaces shown in Figure 21 identify a pre-crack region labeled (1) on the right-hand side of the specimen, whereas (2), (3) and (4) represent the FCG, CFCG and CCG regions respectively. After each test was terminated, the specimen was cooled down and broken open on the servo-hydraulic frame by fatigue at a frequency of 5 to 15 Hz. This minimized the extent of plastic deformation in the remaining ligament of the specimen. A specimen half was then cut to a smaller size on a vertical bandsaw to fit the fracture surface inside of a scanning electron microscope (SEM).

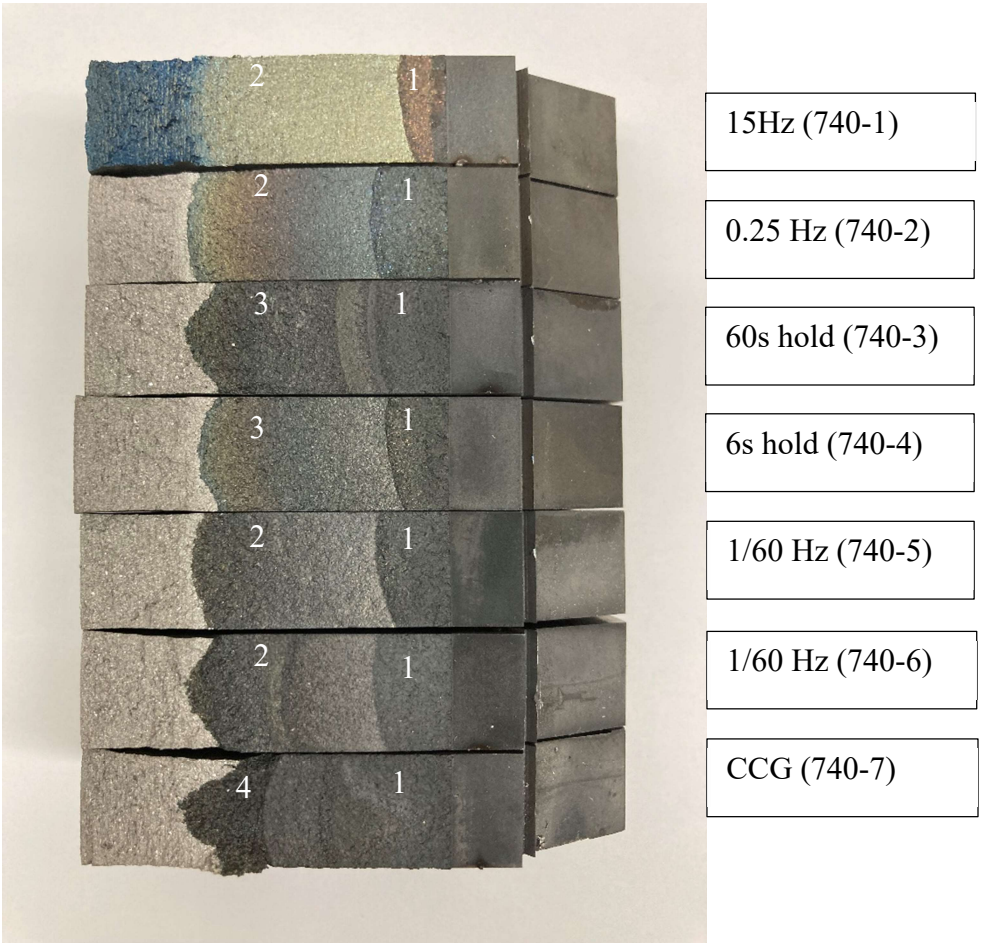

Figure 21: Fracture surfaces of 740H with crack growth from right to left. 1) Pre-crack region, 2) FCG region, 3) CFCG region, 4) CCG region.

All images were taken at an electron high tension of 15 kV with a working distance of 10.0 mm. The 15 Hz test shows a different coloration from other specimens because it broke into two pieces while still at temperature. It should be noted that specimen 740-3 (the 60s hold test) was the only 750℃ test that appeared to have significant crack tunneling as the middle of the crack grew quicker than the sides. Both tests at 800℃ 740-6 and 740-8 also showed significant crack tunneling. The higher amount of crack tunneling seen at 800℃ reveals that the fracture toughness in the middle of the specimen is decreased. This is dictated by the stress state through the thickness of the specimen. For some materials, sidegrooving of the specimen is performed to reduce this effect, but it was not done in this case due to a limited supply of test specimens.

SEM images were taken at the transition from the pre-crack region to the test region as well as at crack lengths corresponding to approximately ΔK=40, 60 and 80 MPa$\sqrt{m}$. Images of the grains in this study were compared to the average grain size of 100 μm which was measured by Zielinski [5] and proved to be similar. This verified that intergranular crack growth was occurring (growth in-between the grains). A similar comparison was made with the fracture surface of creep rupture image provided by Tortorelli [6] which appeared to have a similar surface.

Figure 22 shows crack growth from right to left with an arrow. The approximate transition point is identified (white dashed line) from the room temperature pre-crack to the FCG/CFCG region. The 15 Hz test in Figure 22 (a) showed transgranular growth during pre-crack and during the test. The 0.25 Hz, 6s hold, and 1/60 Hz tests shown in Figure 22 (b), (d), and (e) appeared to have a transition from the pre-crack region (transgranular) to mixed transgranular and intergranular crack growth. The greatest contrast was the transition from

transgranular growth during the pre-crack to intergranular growth shown in Figure 22 (c) for the 60s hold test. This shows that the increased creep effect from the 6s hold to the 60s hold significantly increased the intergranular crack growth of the material. It is reasonable to

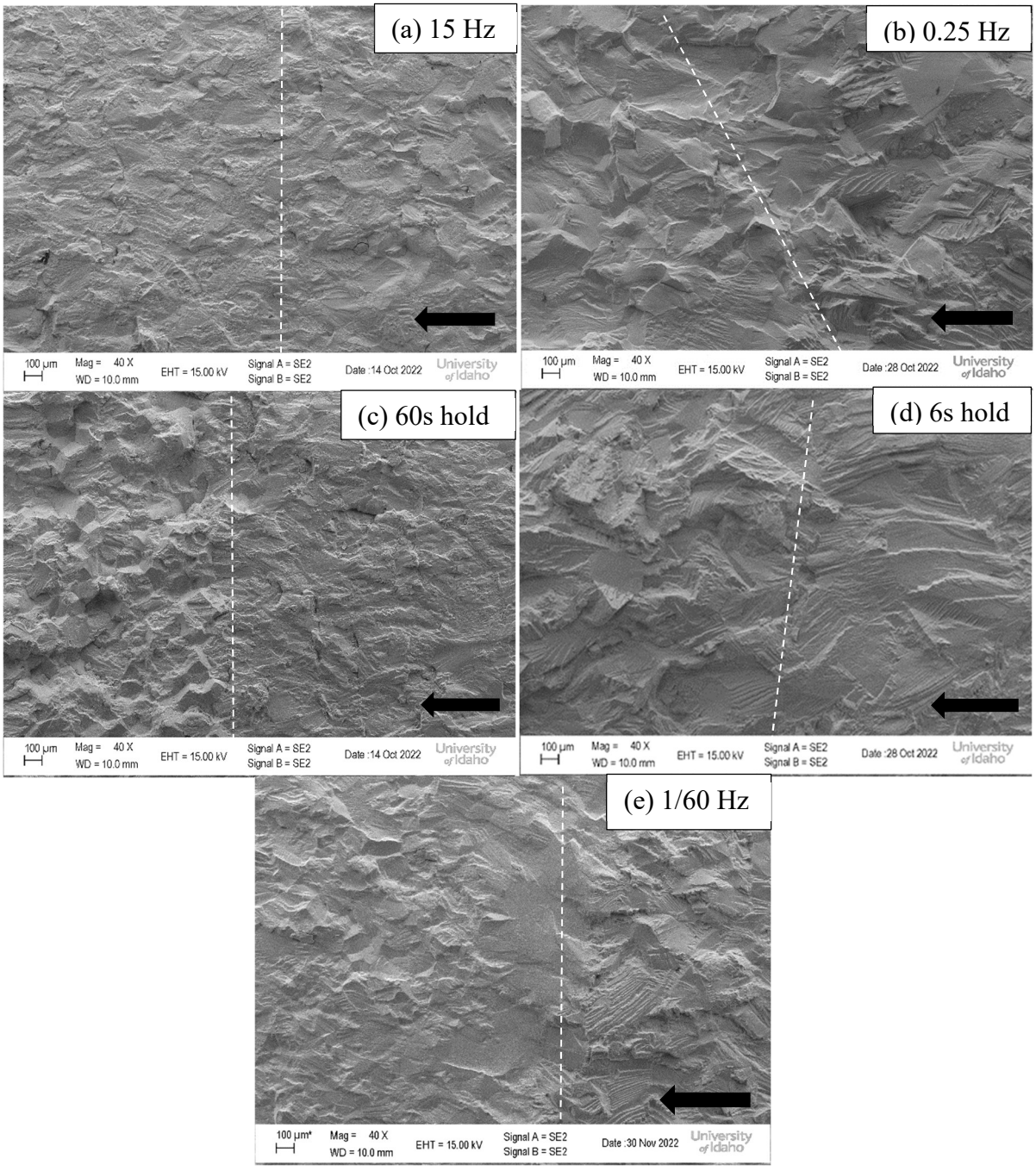

Figure 22: Pre-crack transiton for (a) 15 Hz, (b) 0.25 Hz, (c) 60s hold, (d) 6s hold, (e) 1/60 Hz at 750°C. Crack growth from right to left and pre-crack to crack growth region identified with dotted white line.

assume that the added hold time reduced transgranular cracking and introduced more creep damage into the specimen in the way of intergranular crack growth. A comparison was made at ΔK= 40 MPa$\sqrt{m}$ on the same fracture surfaces. The 15 Hz test in Figure 23 (a) shows transgranular growth throughout whereas the 0.25 Hz and 6s hold tests show mixed

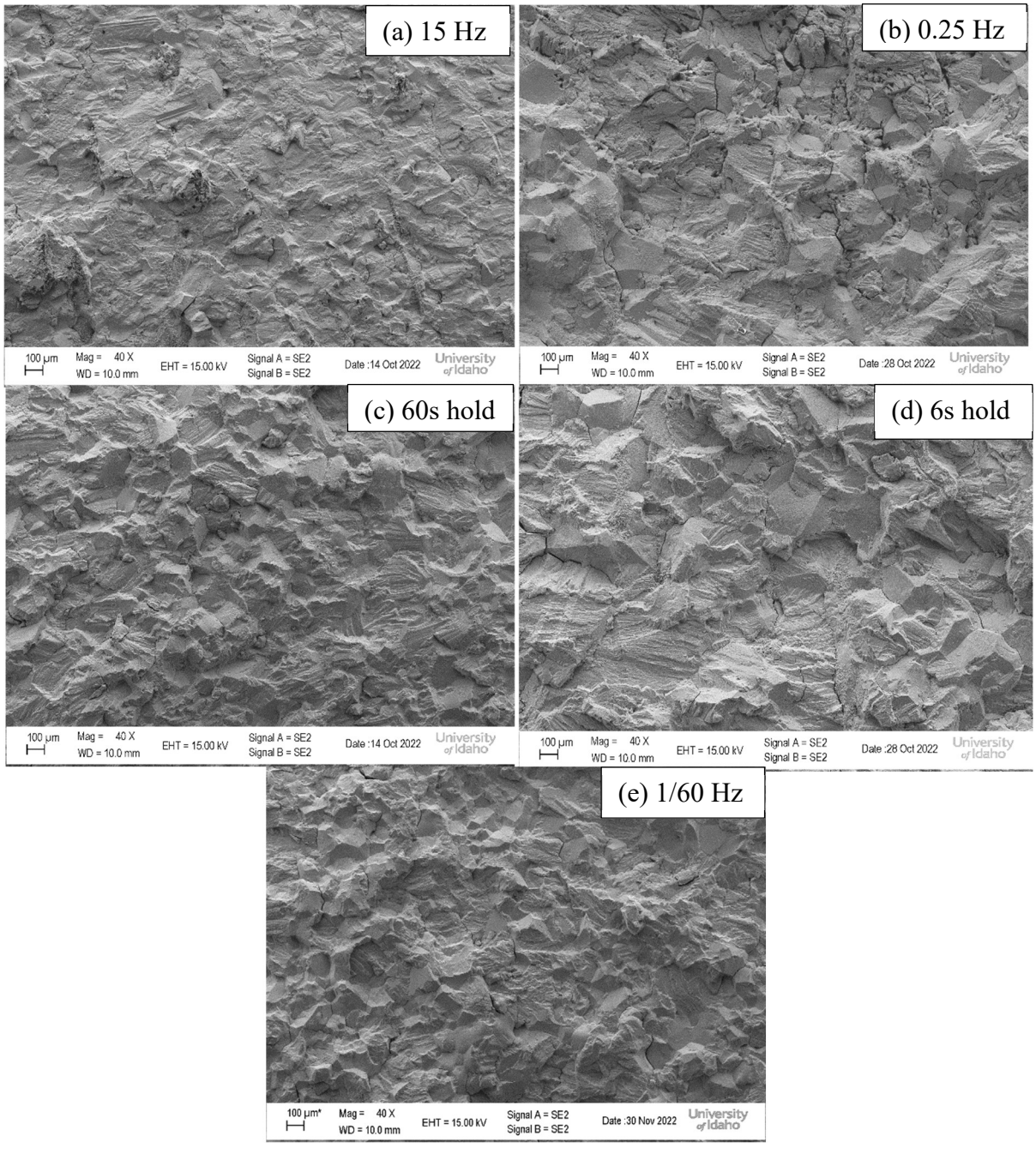

Figure 23: FCG and CFCG fractography at K=40 MPa$\sqrt{m}$ and 750℃.

intergranular and transgranular cracking (striations were observed at higher magnification and verified with the corresponding crack growth rate) in Figure 23 (b) and (d). The 60s hold and 1/60 Hz tests (Figure 23 (c),(e)) were dominated by intergranular crack growth.

Another comparison was made at ΔK=60 MPa$\sqrt{m}$. Figure 24 shows a comparison between the 60s hold and 1/60 Hz tests to better understand the difference in crack growth between the two hold times. Both images show significant intergranular cracking, but the 60s hold show more secondary cracks perpendicular to the fracture plane (secondary cracks shown with arrows).

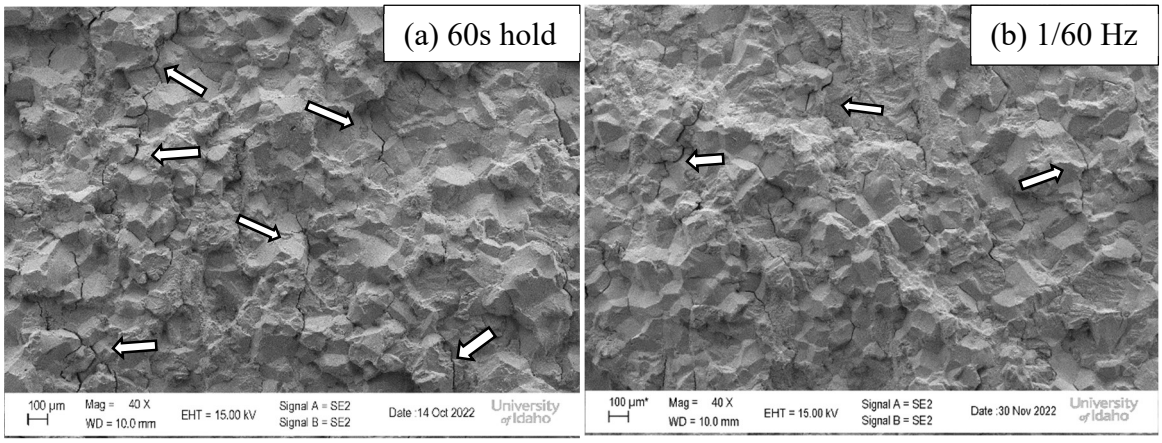

Figure 24: 60s hold vs. 1/60 Hz comparison at ΔK=60 MPa√m and 750°C. White arrows indicate secondary cracking.

To provide a final comparison as the tests approached instability (end of the test), images were taken at ΔK= 80 MPa$\sqrt{m}$ and are shown in Figure 25. Figure 25 (a) shows the 15 Hz test with significant transgranular crack growth (striations were observed at higher magnifications) and limited sign of secondary cracks. The 0.25 Hz and 6s hold tests shown in Figure 25 (b) and (d) both showed intergranular cracking and limited secondary cracking. However, the 0.25 Hz and 6s hold tests also showed striations at higher magnifications

proving transgranular growth (spacing of striations was consistent with the crack growth rate at a given ΔK). Intergranular cracking was dominant for both the 60s hold and 1/60 Hz tests as shown in Figure 25 (c) and (e) with prevalent secondary cracking perpendicular to the fracture plane.

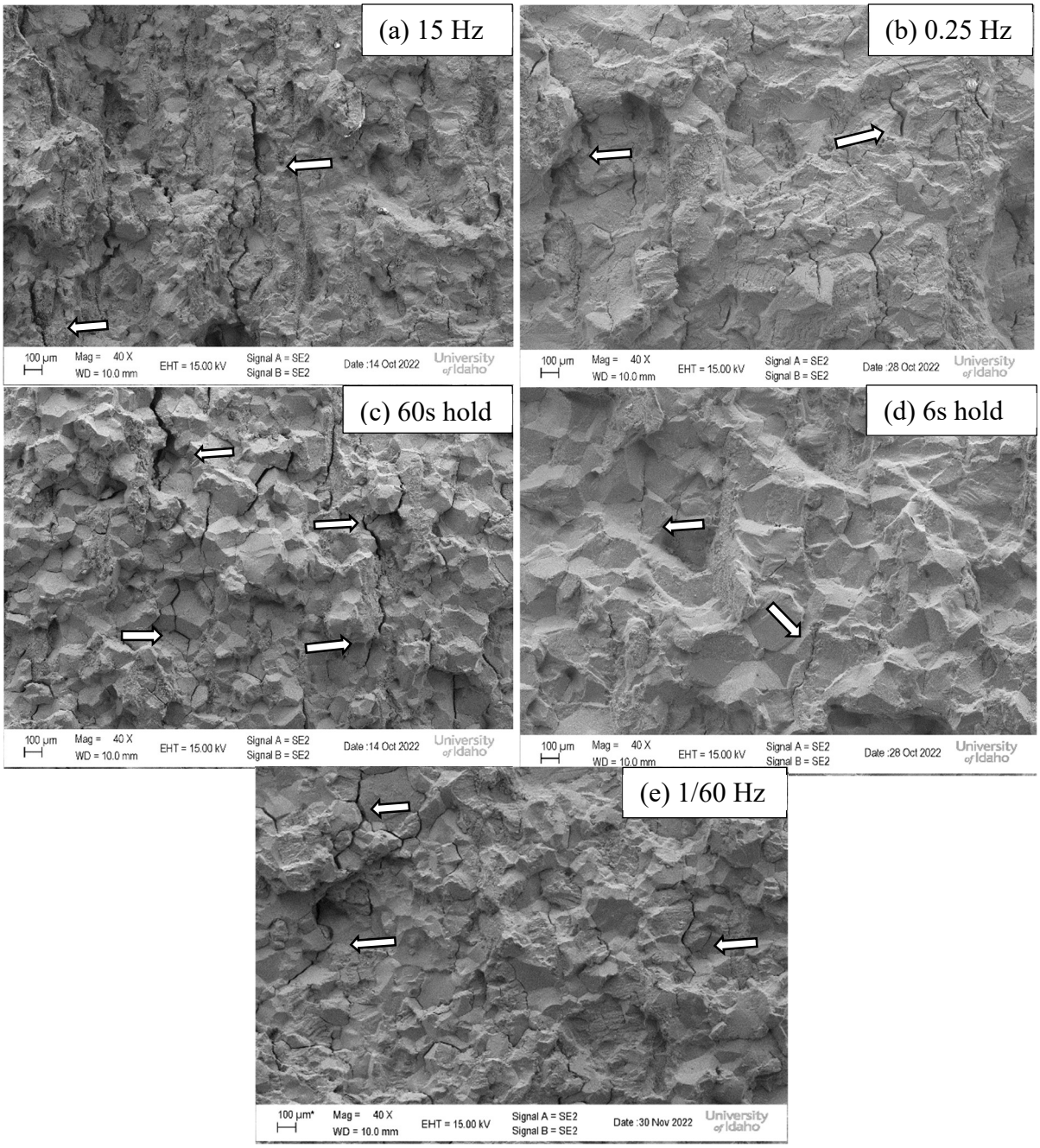

Figure 25: FCG and CFCG fractography at ΔK = 80 MPa$\sqrt{m}$ and 750°C. White arrows indicate secondary cracking.

Comparing the 1/60 Hz and the 60s hold tests, the 60s hold showed more secondary cracks on the fracture surface with more defined grains (showing higher grain boundary decohesion). This phenomenon is potentially attributed to crack-tip blunting where secondary cracks could be reducing the driving force of the crack tip [14]. However, the 6s hold test shows little sign of secondary cracking occurring while also proving to have similar growth to the 60s hold. Repeatability of these tests could help to understand the cause of reduced crack growth rate of the 60s hold time.

While limited tests were performed at 800℃ due to the grip and pin limitations, limited fractography was performed (with the exception of the 60s hold test 740-8). SEM images were taken at the pre-crack transition region and at K_{max} = 66 MPa$\sqrt{m}$. Figure 26 shows the pre-crack transition images for the 1/60 Hz and CCG tests at 800℃ with the approximate transition identified with a dashed white line. The 1/60 Hz test shown in Figure 26 (a) shows pure transgranular growth with no noticeable intergranular cracking. Figure 26 (b) shows the CCG test with an obvious transition from the transgranular pre-crack region to the intergranular CCG region (approximate starting K_{max}=55 MPa$\sqrt{m}$).

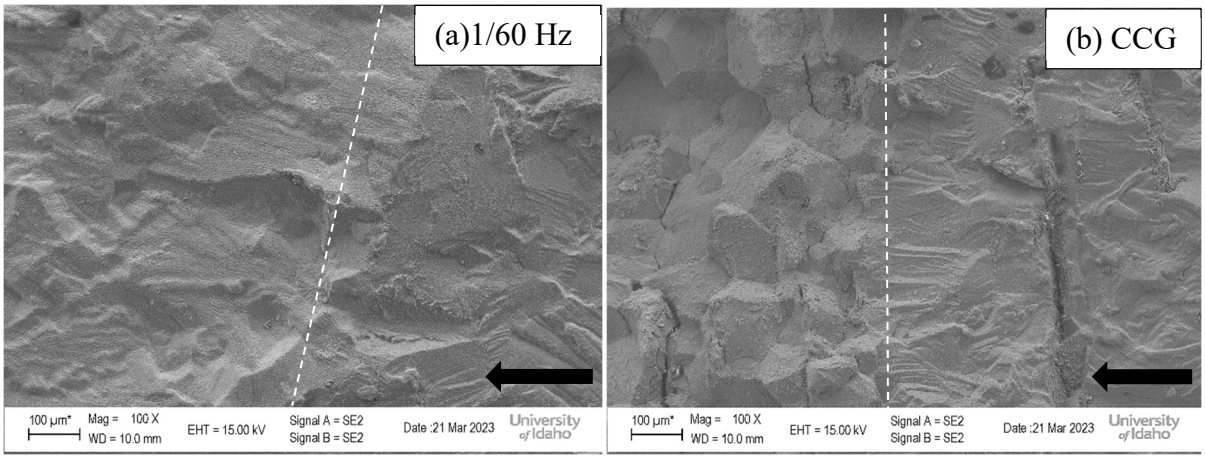

Figure 26: Transition from pre-crack region to test region for (a) 1/60 Hz and (b) CCG at 800°C. Crack growth from right to left and pre-crack to crack growth region identified with dashed white line.

To compare fracture surfaces as the crack grew, images were taken at K_{max}=66 MPa$\sqrt{m}$ as shown in Figure 27. Significant intergranular cracking was observed for both the 1/60 Hz and the CCG tests as shown in Figure 27 (a) and (b). Secondary cracking is evident on both surfaces with a larger number of secondary cracks perpendicular to the surface on the CCG test. The CCG test also shows a more defined granular surface leading to more evidence of grain boundary decohesion and intergranular crack growth.

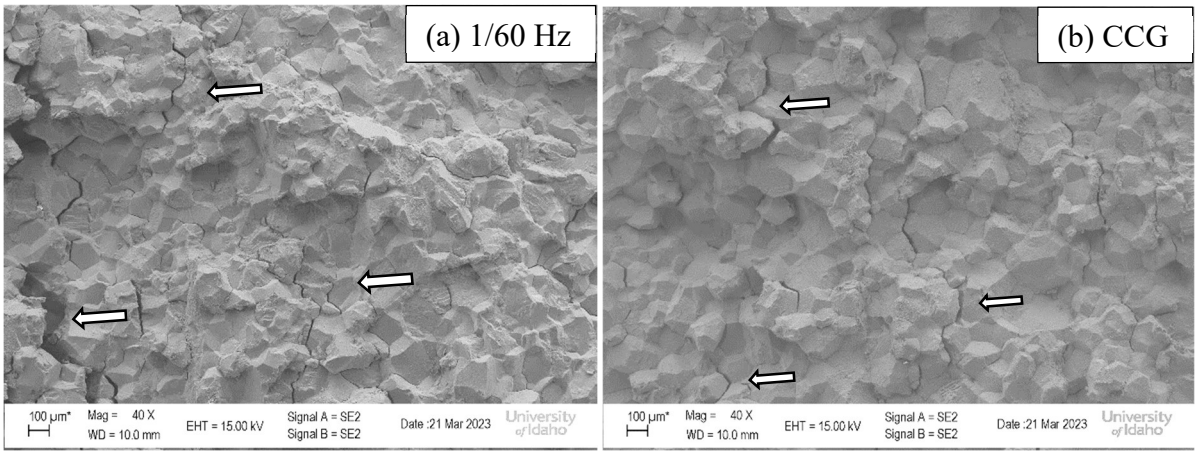

Figure 27: 1/60 Hz vs. CCG comparison at 800℃ for K_{max}=66 MPa$\sqrt{m}$. White arrows indicate secondary cracking.

A comparison was made between 750℃ and 800℃ to understand how the crack growth rate differed for the 1/60 Hz tests. Figure 28 shows the fracture surfaces at a crack length corresponding to approximately ΔK=40 MPa$\sqrt{m}$. At 750℃, there appears to be significantly more intergranular cracking than at 800℃. This behavior was unexpected as

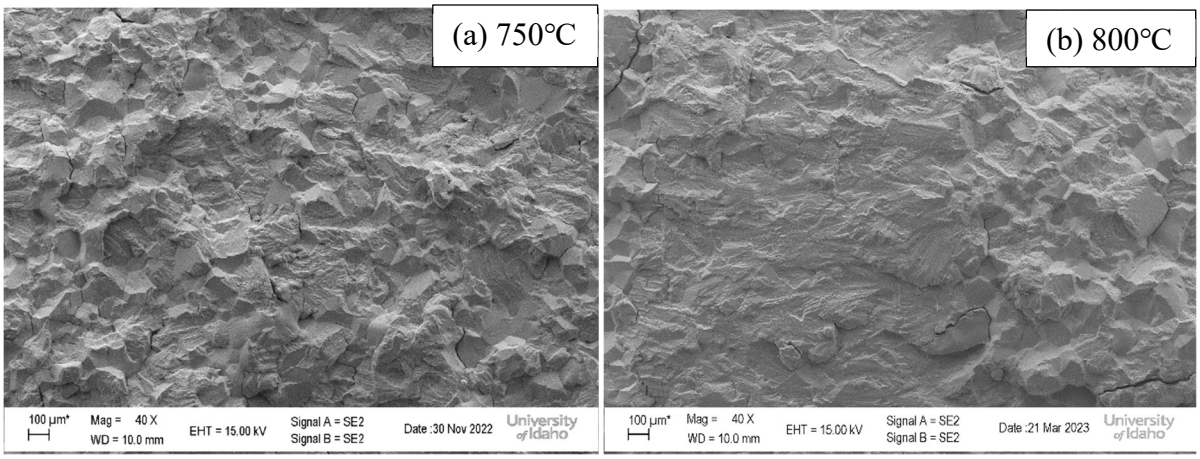

Figure 28: 1/60 Hz temperature comparison at 750°C and 800°C at ΔK=40 MPa$\sqrt{m}$.

raising the temperature would typically increase intergranular cracking. However, at ΔK=60 MPa$\sqrt{m}$, significant intergranular cracking was observed as shown in Figure 29. Secondary cracking perpendicular to the main crack was observed on both surfaces with a similar presence at both temperatures (some wider cracks at 800°C). Fractography temperature comparison in this study appeared similar for 750°C and 800°C.

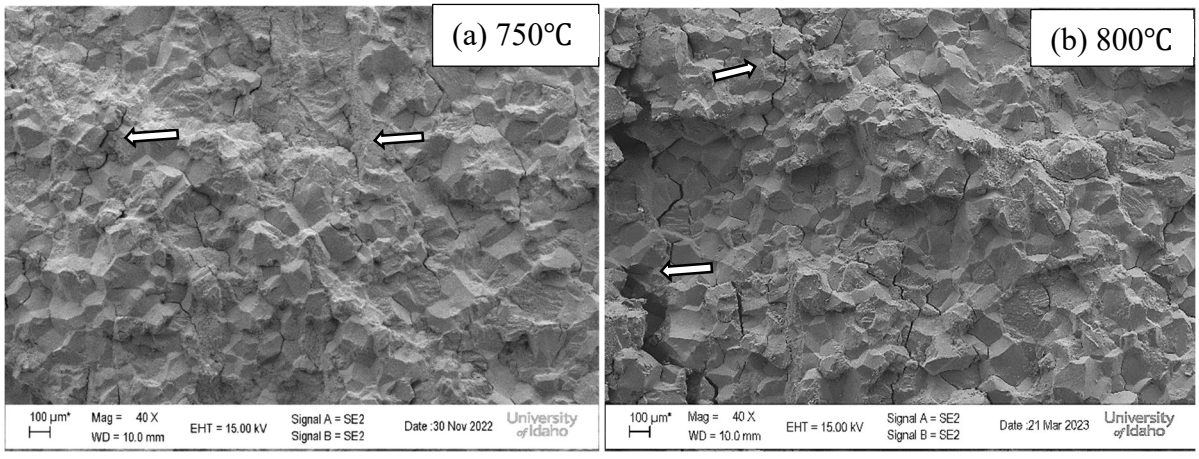

Figure 29: 1/60 Hz temperature comparison at (a) 750°C and (b) 800°C corresponding to ΔK=60 MPa$\sqrt{m}$.

5.) Conclusions and Recommendations

5.1 Conclusions

This study characterized FCG, CFCG and CCG for 740H at elevated temperatures of 750℃ and 800℃. Testing at 750℃ revealed that the crack growth rate (da/dN) as a function of ΔK was similar for all waveforms with the exception of the 1/60 Hz test. Comparing the crack growth rate as a function of time revealed that crack growth in the material is primarily time-independent.

Fractograpy revealed that transgranular crack growth was dominant for the 15 Hz FCG test. All other tests showed either mixed mode (transgranular and intergranular) cracking or primarily intergranular cracking. Significant secondary cracking (perpendicular to the fracture plane) was seen in the 60s hold and 1/60 Hz tests with more secondary cracks and grain boundary decohesion for the 60s hold test. While a hold time typically increases the crack growth rate due to the creep effect, the 1/60 Hz test showed a crack growth rate approximately three times faster for the majority of the test. A possible cause of this phenomenon was crack tip blunting due to the higher number of secondary cracks observed for both the 60s hold and the 6s hold tests.

Comparing 740H to Haynes 282 at 750℃, the 740H data at 15 Hz was similar to the Haynes 282 data for the 25 Hz test. However, when comparing these higher frequencies to a slower frequency of 0.25 Hz, Haynes 282 showed poorer crack growth resistance at the lower frequency whereas 740H showed no noticeable difference. Not only did 740H prove superior at 0.25 Hz, but the slower frequency of 1/60 Hz also showed better crack growth resistance than the 0.25 Hz Haynes 282 test. Comparing CFCG and FCG of 740H to IN617, 740H

proved to be primarily time-independent whereas IN617 showed to be time independent according to Benz [13].

Exploratory FCG and CFCG Testing at 800℃ revealed a higher crack growth rate for the 1/60 Hz test as compared to the 60s hold test (this was the same as the comparison at 750℃). For the single CCG test at 800℃, crack growth was intergranular with a higher amount of secondary cracking than the 1/60 Hz test. A comparison between 750℃ and 800℃ showed that the 1/60 Hz test had little to no change in crack growth rate whereas the 60s hold showed a decrease in crack growth resistance. Fracture surface comparison of the 1/60 Hz frequency showed similar intergranular growth and secondary cracking. It can be reasonably concluded that for 60s hold testing, an increase from 750℃ to 800℃ decreased the crack growth resistance. On the other hand, the 1/60 Hz frequency showed similar crack growth resistance for both temperatures. A possible reason for the decrease in crack growth resistance for the 60s hold test at 800℃ compared to 750℃ is greater grain boundary weakening and thus higher crack growth rates.

5.2 Recommendations and Future Work

This study provides groundwork for understanding FCG and CFCG in 740H at 750℃. However, it should be noted that many problems resulted when increasing the temperature to 800℃ (causing loss of data for the 60s hold and CCG tests). Severe creep deformation occurred in both the grips and pins for the 60s hold and CCG tests (both tests were being performed simultaneously). Given the reduced creep performance of the grip and pin material at 800℃, a different material is required for future testing. As a result, fixtures made of Waspalloy were recently fabricated by EPRI to continue the 800℃ work at the University of Idaho.

While this study gave a baseline for FCG, CFCG and CCG testing on 740H, there are several areas of interest for future work. Due to the termination of the 60s hold test at 800℃, no fractography was completed. Performing a complete 60s hold test at 800℃ would allow for a valid comparison to 750℃ regarding fractography and crack growth. While some conclusions were drawn on FCG and CFCG testing for 740H, little is known about long term CCG testing. CCG testing at 700℃ would allow for a material comparison to C-263 and IN617 as researched by Mueller [19]. A long-term CCG and a 600s hold test at 750℃ and 800℃ would allow for comparison between all FCG and CFCG testing performed in this study. These tests could provide more insight on the formation of secondary cracking during creep performance and could further validate crack-tip blunting as a mode of CCG resistance. Further exploration in interrupted CCG testing (300hr, 600hr, 1000hr) would open opportunities for characterizing creep damage below the surface of the crack which was not explored in this study.

6.) References

[1] Iea. (2022, December 16). *Coal - fuels & technologies*. IEA. Retrieved March 28, 2023, from https://www.iea.org/fuels-and-technologies/coal

[2] *Advanced ultra-supercritical technology: GE Steam Power*. gepowersteam.(n.d.).Retrieved March 28, 2023, from https://www.ge.com/steam-power/coal-power-plant/usc-ausc

[3] Shingledecker, J. P., & Pharr, G. M. (2012). The role of ETA phase formation on the creep strength and ductility of inconel alloy 740 at 1023 K (750 °C). *Metallurgical and Materials Transactions A*, *43*(6), 1902–1910. https://doi.org/10.1007/s11661-011-1013-4

[4] PCC Energy Group. (n.d.). *INCONEL ALLOY 740H A Superalloy Specifically Designed For Advanced Ultra Supercritical Power Generation*. Retrieved February 6, 2023, from https://www.specialmetals.com/documents/technical-bulletins/inconel/inconel-alloy-740h.pdf

[5] Zieliński, A., Sroka, M., & Dudziak, T. (2018, October 30). *Microstructure and mechanical properties of Inconel 740H after long-term service*. Materials (Basel, Switzerland). Retrieved Janhttps://www.ncbi.nlm.nih.gov/pmc/articles/PMC6265915/#:~:text=The%20measured%20average%20grain%20diameter,that%20in%20the%20ASTM%20cards).&text=Microstructure

[6] Tortorelli, P. F., Wang, H., Unocic, K. A., Santella, M. L., Shingledecker, J. P., & Cedro, V. (2014). Long-Term Creep-Rupture Behavior of Inconel® 740 and Haynes® 282. *ASME 2014 Symposium on Elevated Temperature Application of Materials for Fossil, Nuclear, and Petrochemical Industries*, 29–36. https://doi.org/10.1115/ETAM2014-1003

[7] R. Stephens, A. Fatemi, R. Stephens, and H. Fuchs, Metal Fatigue in Engineering, Second. Wiley-Interscience, 2001.

[8] Rountree, C., Kalia, R., Lidorikis, E., Nakano, A., Van Brutzel, L., & Vashishta, P. (2002). Atomistic Aspects of Crack Propagation in Brittle Materials: Multimillion Atom Molecular Dynamics Simulations. *Annu. Rev. Mater. Res*, *12*, 377–400. https://doi.org/10.1146/annurev.matsci.32.111201.142017

[9] ASTM. (1996). *Annual book of ASTM standards. Section 3, metals test methods and analytical procedures*.

[10] Ulbrich. (2022). *Haynes 282 alloy*. https://www.ulbrich.com/. Retrieved March 27, 2023, from https://haynesintl.com/docs/default-source/pdfs/new-alloy-brochures/high-temperature-alloys/brochures/282-brochure.pdf?sfvrsn=20

[11] Rozman, K. A., Kruzic, J. J., & Hawk, J. A. (2015). Fatigue Crack Growth Behavior of Nickel-base Superalloy Haynes 282 at 550-750° C. Journal of Materials Engineering and Performance, 24(8), 2841-2846. doi:10.1007/s11665-015-1588-9

[12] *www.specialmetals*. (n.d.). Retrieved March 28, 2023, from https://www.specialmetals.com/documents/technical-bulletins/inconel/inconel-alloy-617.pdf

[13] Benz, J. K., & Wright, R. N. (n.d.). Fatigue and Creep Crack Propagation Behaviour of Alloy 617 in the Annealed and Aged Conditions. INL.

[14] A. Saxena, Nonlinear Fracture Mechanics for Engineers, First. CRC Press, 1998.

[15] A. T. Yokobori Jr., "Difference in the creep and creep crack growth behavior between creep ductile and creep brittle materials," Engineering Fracture Mechanics, vol. 62, no. 1, pp. 61-78, 1999.

[16] *Solution annealing heat treatment for various metals*. Bluewater Thermal Solutions. (n.d.). Retrieved February 1, 2023, from https://bluewaterthermal.com/solution-annealing-heat-treatment/

[17] Saxena, A. (2015). Creep and creep–fatigue crack growth. *International Journal of Fracture*, *191*(1-2), 31–51. https://doi.org/10.1007/s10704-015-9994-4

[18] Chen, K., Dong, J., & Yao, Z. (2021). Creep Failure and Damage Mechanism of Inconel 718 Alloy at 800–900 °C. *Metals and Materials International*, *27*(5), 970–984. https://doi.org/10.1007/s12540-019-00447-4

[19] Joint EPRI – 123HiMAT International Conference on Advances in High Temperature Materials October 21–24, 2019, Nagasaki, Japan J. Shingledecker, M. Takeyama, editors

[20] Shaber, N. L., & Stephens, R. R. (2018). *Investigation of fatigue and creep-fatigue crack growth in Alloy 709 at elevated temperatures*. University of Idaho.

[21] Gibson, C. J. (2021). *Creep Fatigue Crack Growth Behavior of Wrought and Additive Manufactured IN718 at Elevated Temperature*. ProQuest Dissertations Publishing.

7.) Appendices

A.1 Specimen 740-1 (15Hz and T=750℃)))

a(mm)	caliper(mm)	Cycles	Time	Pmax(lbs)	Pmin(lbs)	DCPD(mV)
15.32	17.85	1000	9:28	2476	248	0.2278
15.82	18.35	13700	9:42	2476	248	0.2426
17.61	20.14	29600	9:59	2476	248	0.2689
17.91	20.44	32000	10:02	2476	248	0.2757
18.12	20.65	34000	10:05	2476	248	0.2805
18.42	20.95	36000	10:07	2476	248	0.2834
18.72	21.25	39000	10:11	2476	248	0.2909
19.02	21.55	41000	10:13	2476	248	0.2947
19.32	21.85	43000	10:15	2476	248	0.2994
19.62	22.15	45000	10:17	2476	248	0.3049
19.92	22.45	46600	10:18	2476	248	0.3077
20.22	22.75	48000	10:20	2476	248	0.3111
20.52	23.05	49000	10:22	2476	248	0.3152
20.82	23.35	53000	10:25	2476	248	0.3238
21.57	24.1	57000	10:30	2476	248	0.3379
21.87	24.4	59000	10:32	2476	248	0.3434
22.17	24.7	60000	10:34	2476	248	0.3478
22.47	25	61000	10:35	2476	248	0.3512
22.77	25.3	64000	10:38	2476	248	0.3607
23.07	25.6	66000	10:40	2476	248	0.3687
23.37	25.9	67000	10:41	2476	248	0.3709
23.67	26.2	68000	10:42	2476	248	0.378
24.22	26.75	71000	10:46	2476	248	0.389
24.99	27.52	72000	10:47	2476	248	0.3985
25.27	27.8	74000	10:49	2476	248	0.403
25.57	28.1	75000	10:50	2476	248	0.4092
26.27	28.8	76000	10:51	2476	248	0.417
27.07	29.6	78000	10:54	2476	248	0.4303
28.28	30.81	80000	10:58	2476	248	0.469
29.04	31.57	83000	10:59	2476	248	0.4729
30.82	32.8	84000	11:00	2476	248	0.4859
test stopped and frequency slowed down to 10 Hz						
36.94	40.83	890000	11:32	2476	248	0.6318

A.2 Specimen 740-2 (0.25Hz and T=750℃))

a(mm)	caliper(mm)	Cycles	Time	Date	Pmax(lbs)	Pmin(lbs)	DCPD(mV)
18	21.36	50	8:23	11-May	2078	211	0.281
18.11	21.47	4272	13:07	11-May	2078	211	0.288
18.77	22.13	5368	14:20	11-May	2078	211	0.29
19.02	22.38	6038	15:05	11-May	2078	211	0.292
n/a	n/a	7211	16:23	11-May	2078	211	0.2957
19.35	22.8	8537	17:50	11-May	2078	211	0.2989
19.55	23	9636	19:04	11-May	2078	211	0.303
19.76	23.21	11100	20:40	11-May	2078	211	0.3074
20.31	23.76	13628	23:29	11-May	2078	211	0.3142
21.55	25	20221	6:48	12-May	2078	211	0.3358
22.18	25.63	22898	9:46	12-May	2078	211	0.346
22.48	25.93	23970	10:57	12-May	2078	211	0.3508
22.74	26.19	25092	12:12	12-May	2078	211	0.355
23.3	26.75	26171	13:23	12-May	2078	211	0.3603
23.72	27.17	27947	15:22	12-May	2078	211	0.3689
24.07	27.52	28975	16:30	12-May	2078	211	0.375
24.2	27.65	29639	17:14	12-May	2078	211	0.3781
24.66	28.11	30651	18:21	12-May	2078	211	0.3827
25.29	28.74	32035	19:53	12-May	2078	211	0.3903
25.7	29.15	33926	21:59	12-May	2078	211	0.4056
26.62	30.07	35479	23:43	12-May	2078	211	0.417
27.75	31.2	37543	2:00	13-May	2078	211	0.433
28.52	31.97	38209	2:44	13-May	2078	211	0.44
28.85	32.3	n/a	n/a	13-May	2078	211	n/a
29.4	32.85	40149	4:53	13-May	2078	211	0.463
30.48	33.93	40820	5:38	13-May	2078	211	0.472
30.6	34.05	41460	6:20	13-May	2078	211	0.4825
30.36	34.35	41889	6:49	13-May	2078	211	0.49
n/a	n/a	42511	7:30	13-May	2078	211	0.502
31.06	35.05	42999	8:03	13-May	2078	211	0.514
31.61	35.6	43199	n/a	13-May	2078	211	0.519
31.76	35.75	43336	8:25	13-May	2078	211	0.52
31.86	35.85	43576	8:41	13-May	2078	211	0.527
33.2	36.65	43961	9:07	13-May	2078	211	0.538
33.4	36.85	44289	9:28	13-May	2078	211	0.548
33.95	37.4	44503	9:43	13-May	2078	211	0.556
34.12	37.57	44756	9:59	13-May	2078	211	0.567
34.76	38.21	44997	10:15	13-May	2078	211	0.579

35.05	38.5	45103	10:22	13-May	2078	211	0.587
35.35	38.8	45145	10:25	13-May	2078	211	0.589
35.65	39.1	45285	10:35	13-May	2078	211	0.6
n/a	n/a	45441	10:45	13-May	2078	211	0.614
n/a	n/a	45540	10:51	13-May	2078	211	0.625
n/a	n/a	45576	10:54	13-May	2078	211	0.63
n/a	n/a	45640	n/a	13-May	2078	211	0.646
n/a	n/a	45664	11:00	13-May	2078	211	0.656

A.3 Specimen 740-3 (60s Hold and T=750℃))

a(mm)	caliper(mm)	Cycles	Time	Date	Pmax(lbs)	Pmin(lbs)	DCPD(mV)
18.66	20.16	10323	12:15	18-Jul	2280	228	0.2835
18.97	20.47	11591	9:23	19-Jul	2280	228	0.2983
19.07	20.57	13133	11:06 AM	20-Jul	2280	228	0.2986
Little to no crack growth. Load is being bumped 10%							
19.11	20.62	14644	12:16 PM	21-Jul	2500	250	0.2975
19.31	20.81	18218	11:51 PM	23-Feb	2500	250	0.3
19.45	20.9	20334	11:10 AM	25-Jul	2500	250	0.301
19.57	21.02	23226	11:22 AM	27-Jul	2500	250	0.304
19.8	21.25	29703	11:19 PM	31-Jul	2500	250	0.282
19.91	21.36	33203	9:39 AM	3-Aug	2500	250	0.281
19.95	21.4	36140	10:55 AM	5-Aug	2500	250	0.284
Little to no crack growth. Load is being bumped 10%, test cycled at 15 Hz to initiate crack growth, N=11,892 cycles were added when cycling the specimen.							
21.9	23.35	48032	11:38 AM	5-Aug	2750	275	0.319
22.25	23.55	N/A	N/A	N/A	2750	275	N/A
N/A	N/A	49485	11:49 AM	6-Aug	2750	275	0.325
22.75	24.05	52169	8:35 AM	8-Aug	2750	275	0.335
23.25	24.55	53656	9:22 AM	9-Aug	2750	275	0.339
23.75	25.05	55414	2:40 PM	10-Aug	2750	275	0.346
Controller shut off due to power outage at N=56931 cycles.							
24.25	25.55	56975	9:29 AM	12-Aug	2750	275	0.352
24.87	26.17	60086	1:20 PM	14-Aug	2750	275	0.367
25.37	26.67	61403	11:22 AM	15-Aug	2750	275	0.371
25.65	26.95	62706	9:02 PM	16-Aug	2750	275	0.38
26.65	27.95	64141	8:55 AM	17-Aug	2750	275	0.388
26.7	28	65543	8:17 AM	18-Aug	2750	275	0.399
27.1	28.4	66467	11:41 PM	18-Aug	2750	275	0.406
27.5	28.8	67046	9:20 AM	19-Aug	2750	275	0.412
28.4	29.7	68726	1:20 PM	20-Aug	2750	275	0.43

29.5	30.8	70087	12:01 PM	21-Aug	2750	275	0.449
30.1	31.4	70671	9:45 PM	21-Aug	2750	275	0.4605
31.05	32.35	71449	10:43 AM	22-Aug	2750	275	0.481
31.56	32.86	71716	3:10 PM	22-Aug	2750	275	0.491
32.7	34	72157	10:32 PM	22-Aug	2750	275	0.515
33.15	34.45	72263	12:18 AM	23-Aug	2750	275	0.522
Test Paused at N=72265 cycles.							
33.15	34.45	72267	8:01 AM	23-Aug	2750	275	N/A
34.32	35.62	72439	10:52 AM	23-Aug	2750	275	0.546
34.7	36	72519	12:13 PM	23-Aug	2750	275	0.56
35.2	36.5	72537	12:30 PM	23-Aug	2750	275	0.574
35.35	36.65	72543	12:37 PM	23-Aug	2750	275	0.586
35.65	36.95	72545	12:41 PM	23-Aug	2750	275	0.621

A.4 Specimen 740-4 (6s Hold and T=750℃))

a(mm)	caliper(mm)	Cycles	Time	Date	Pmax(lbs)	Pmin(lbs)	DCPD(mV)
17.48	20.42	0	10:43 AM	6-Sep	2068	207	0.1909
17.67	20.61	13717	9:39 AM	7-Sep	2068	207	0.202
Little to no crack growth. Load bumped 10% and crack is grown 1 mm at 10 Hz to initiate growth.							
18.82	22.15	N/A	N/A	N/A	2287	229	N/A
18.82	22.15	N/A	3:12 PM	8-Sep	2287	229	0.2022
Little to no crack growth. Load bumped 10% and crack is grown 1 mm at 10 Hz to initiate growth							
19.32	22.65	73329	11:32 AM	11-Sep	2500	250	0.2149
19.97	23.3	86578	9:37 AM	12-Sep	2500	250	0.228
20.37	23.7	95122	11:51 PM	12-Sep	2500	250	0.243
21.97	25.3	101262	10:09 AM	13-Sep	2500	250	0.254
21.97	25.3	109507	11:50 PM	13-Sep	2500	250	0.272
22.9	26.45	115945	10:34 AM	14-Sep	2500	250	0.286
23.45	27	119974	5:00 PM	14-Sep	2500	250	0.297
N/A	N/A	123360	10:55 PM	14-Sep	2500	250	0.304
24.75	28.3	130178	10:17 AM	14-Sep	2500	250	0.331
25.2	28.75	132972	2:56 PM	15-Sep	2500	250	0.342
26	29.55	137088	9:48 PM	15-Sep	2500	250	0.364
29.3	32.85	144004	9:19 AM	16-Sep	2500	250	0.423
30.95	34.5	146339	1:13 PM	16-Sep	2500	250	0.457
32.25	35.8	147414	3:00 PM	16-Sep	2500	250	0.483
34.3	37.85	148239	4:23 PM	16-Sep	2500	250	0.505
35.15	38.7	148422	16:43	16-Sep	2500	250	0.513
35.9	39.45	148760	5:15 PM	16-Sep	2500	250	0.538
N/A	N/A	148872	5:26 PM	16-Sep	2500	250	0.554

A.5 Specimen 740-5 (1/60 Hz and T=750℃)

a(mm)	caliper(mm)	Cycles	Time	Date	Pmax(lbs)	Pmin(lbs)	DCPD(mV)
18	20.35	12	4:36 PM	8-Oct	2067	206	0.225
18.65	21.5	22892	1:58 PM	24-Oct	2067	206	0.242
Load bumped 10% higher							
18.65	21.5	27299	3:29 PM	27-Oct	2275	228	0.244
18.95	21.8	32743	10:12 AM	31-Oct	2275	228	0.258
19.37	22.22	34381	1:30 PM	1-Nov	2275	228	0.264
19.65	22.5	35674	11:04 AM	2-Nov	2275	228	0.2649
19.85	22.7	37110	11:00 AM	3-Nov	2275	228	0.271
Computer Shutoff data collection re-started							
20.4	23.25	38690	1:19 PM	4-Nov	2275	228	0.2774
Test re-started due to power outage							
21	23.85	41523	11:19 AM	7-Nov	2275	228	0.287
21.35	24.2	42917	9:36 AM	8-Nov	2275	228	0.302
22.05	24.9	44476	12:32 PM	9-Nov	2275	228	0.311
22.47	25.32	46014	2:10 PM	10-Nov	2275	228	0.318
23.15	26	47286	10:23 AM	11-Nov	2275	228	0.322
23.7	26.55	48826	12:04 PM	12-Nov	2275	228	0.3342
24.65	27.5	50849	9:50 PM	13-Nov	2275	228	0.353
25.47	28.32	52192	9:09 PM	14-Nov	2275	228	0.371
26.14	28.99	53113	12:30 PM	15-Nov	2275	228	0.384
27.65	30.5	54794	4:31 PM	16-Nov	2275	228	0.403
29	31.85	56194	3:51 PM	17-Nov	2275	228	0.423
30.6	33.45	57291	10:09 AM	18-Nov	2275	228	0.455
N/A	N/A	57478	12:15 PM	18-Nov	2275	228	0.462
38.65	41.5	59050	2:28 PM	19-Nov	2275	228	0.595

A.6 Specimen 740-6 (1/60 Hz and T=800℃)

a(mm)	caliper(mm)	Cycles	Time	Date	P_{max}(lbs)	P_{min}(lbs)	DCPD(mV)
18	21.35	8	1:12 PM	10-Dec	2270	227	0.28
18.8	22.15	2172	1:14 AM	12-Dec	2270	227	0.285
19.08	22.43	3150	4:35 PM	12-Dec	2270	227	0.289
19.3	22.65	4212	10:17 AM	13-Dec	2270	227	0.293
19.7	23.05	5789	12:34 PM	14-Dec	2270	227	0.3
20.1	23.45	7096	11:21 AM	15-Dec	2270	227	0.305
20.67	24.02	8511	9:56 AM	16-Dec	2270	227	0.314
21.25	24.6	10079	12:00 PM	17-Dec	2270	227	0.3238

21.75	25.1	11704	3:10 PM	18-Dec	2270	227	0.336
22.32	25.67	12819	9:42 AM	19-Dec	2270	227	0.346
23.4	26.75	14297	10:27 AM	20-Dec	2270	227	0.36
24.16	27.51	15725	10:14 AM	21-Dec	2270	227	0.376
26.75	30.1	17420	2:30 PM	22-Dec	2270	227	0.405
28.25	31.6	18778	1:00 PM	23-Dec	2270	227	0.434
Test Paused for keycard accees issues							
n/a	n/a	18786	10:36 AM	26-Dec	2270	227	0.4
n/a	n/a	20188	10:00 AM	27-Dec	2270	227	0.407
n/a	n/a	21592	9:26 AM	28-Dec	2270	227	0.413
29.05	32.4	23035	9:20 AM	29-Dec	2270	227	0.423
29.78	33.13	24479	9:35 AM	30-Dec	2270	227	0.433
Test shutoff heating element broke							
Test Re-started							
n/a	n/a	24648	10:35 AM	7-Jan	2270	227	0.496
35.55	38.9	25541	1:30 AM	8-Jan	2270	227	0.602

A.7 Specimen 740-7 (CCG and T=800℃)

a(mm)	Date	Time	Dial 1 (in.)	Dial 2 (in.)	P(lbs)	Angle(°)	DCPD(mv)
29.6	8-Feb	3:03 PM	0	0	2710	-1.3	0.481
N/A	9-Feb	10:52 AM	0.02	0.025	2710	-2.6	0.48
N/A	10-Feb	9:20 AM	0.04	0.05	2710	-4.1	0.48
N/A	11-Feb	12:18 AM	0.06	0.07	2710	-5.3	0.481
N/A	11-Feb	9:35 AM	0.07	0.08	2710	-6	0.48
N/A	11-Feb	11:51 PM	0.09	0.1	2710	-7.4	0.481
N/A	12-Feb	8:14 AM	0.11	0.115	2710	-8.3	0.481
N/A	12-Feb	11:02 PM	0.122	0.135	2710	-9.6	0.481
Angle maxed out. Angle re-adjusted and dial indicators re-zeroed.							
30.25	13-Feb	4:57 PM	0	0	2710	11	0.492
30.25	13-Feb	11:23 PM	0.012	0.012	2710	10.4	0.493
30.25	14-Feb	9:12 AM	0.03	0.029	2710	9.6	0.494
30.35	14-Feb	4:40 PM	0.044	0.041	2710	9	0.494
30.35	14-Feb	8:37 PM	0.05	0.048	2710	8.7	0.495
30.43	15-Feb	10:26 AM	0.079	0.076	2710	7.3	0.512
31.12	15-Feb	11:29 PM	0.106	0.105	2710	5.9	0.499
31.6	16-Feb	9:00 AM	0.132	0.13	2710	4.5	0.503
31.6	16-Feb	4:25 PM	0.152	0.152	2710	3.5	0.506
n/a	17-Feb	9:19 AM	N/A	N/A	2710	-9.5	0.58

A.8 Specimen 740-8 (60s hold and T=800℃)

a(mm)	caliper(mm)	Cycles	Time	Date	Pmax(lbs)	Pmin(lbs)	DCPD(mv)
22.4	14.67	0	10:50 AM	15-Feb	2702	270	0.327
22.73	15	384	5:13 PM	15-Feb	2702	270	0.335
23.18	15.45	757	11:27 PM	15-Feb	2702	270	0.341
23.53	15.8	1333	9:00 AM	16-Feb	2702	270	0.348
23.63	15.9	1777	4:25 PM	16-Feb	2702	270	0.352
23.7	15.97	2129	10:17 PM	16-Feb	2702	270	0.354
24.15	16.42	2868	10:38 AM	16-Feb	2702	270	0.36
25.18	17.45	5414	5:01 AM	18-Feb	2702	270	0.386
Displacement Lock hit. Test re-started							
25.68	17.95	6447	10:52 PM	19-Feb	2702	270	0.397
25.83	18.1	7038	8:44 AM	20-Feb	2702	270	0.403
Displacement Lock hit. Test re-started							
26.7	N/A	7687	11:09 PM	20-Feb	2702	270	0.418
Pin sheared							

A.9 Example Load Shedding Procedure

a (mm)	**α**	**F(α)**	**ΔP (kN)**	**ΔP (kips)**	**P_{max} (kips)**	**P_{min} (kips)**	**ΔK (MPa√m)**	**K_{max} (MPa√m)**	**K_{min} (MPa√m)**
10.2	0.201	4.289	22.670	5.096	5.663	0.566	34.000	37.778	3.778
10.5	0.207	4.364	21.654	4.868	5.409	0.541	33.047	36.719	3.672
11	0.217	4.491	20.436	4.594	5.105	0.510	32.094	35.660	3.566
11.5	0.227	4.619	19.280	4.334	4.816	0.482	31.141	34.601	3.460
12	0.237	4.748	18.182	4.087	4.542	0.454	30.188	33.542	3.354
12.5	0.247	4.879	17.136	3.852	4.280	0.428	29.235	32.483	3.248
13	0.256	5.011	16.140	3.628	4.032	0.403	28.281	31.424	3.142
13.5	0.266	5.145	15.189	3.415	3.794	0.379	27.328	30.365	3.036
14	0.276	5.281	14.281	3.211	3.567	0.357	26.375	29.306	2.931
14.5	0.286	5.420	13.413	3.015	3.350	0.335	25.422	28.247	2.825
15	0.296	5.561	12.583	2.829	3.143	0.314	24.469	27.188	2.719
15.5	0.306	5.705	11.788	2.650	2.944	0.294	23.516	26.129	2.613
16	0.316	5.851	11.026	2.479	2.754	0.275	22.563	25.070	2.507
16.5	0.325	6.002	10.296	2.315	2.572	0.257	21.610	24.011	2.401
17	0.335	6.155	9.596	2.157	2.397	0.240	20.657	22.952	2.295
17.5	0.345	6.313	8.925	2.006	2.229	0.223	19.704	21.893	2.189
18	0.355	6.475	8.281	1.862	2.068	0.207	18.750	20.834	2.083